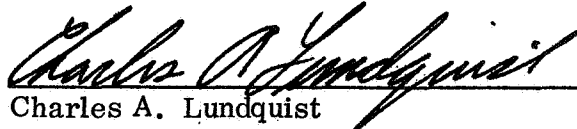NASA CONTRACTOR
REPORT

NASA CR-144162

DIMENSIONAL STABILITY

By Robert Hochen and Ben Justice
Corning Glass Works
Corning, New York

February 1976

Prepared for

NASA – GEORGE C. MARSHALL SPACE FLIGHT CENTER
Marshall Space Flight Center, Alabama   35812

1. REPORT NO. NASA CR-144162	2. GOVERNMENT ACCESSION NO.	3. RECIPIENT'S CATALOG NO.
4 TITLE AND SUBTITLE Dimensional Stability		5. REPORT DATE February 1976
		6. PERFORMING ORGANIZATION CODE
7. AUTHOR(S) Robert Hochen and Ben Justice		8. PERFORMING ORGANIZATION REPORT #
9. PERFORMING ORGANIZATION NAME AND ADDRESS Corning Glass Works Corning, New York		10. WORK UNIT NO.
		11. CONTRACT OR GRANT NO. NAS8-28662
		13. TYPE OF REPORT & PERIOD COVERED
12. SPONSORING AGENCY NAME AND ADDRESS National Aeronautics and Space Administration Washington, D. C. 20546		Contractor June 1972 to October 1975
		14. SPONSORING AGENCY CODE

15. SUPPLEMENTARY NOTES

Prepared for the Space Sciences Laboratory, NASA-Marshall Space Flight Center

16. ABSTRACT

The temporal stability of glass and glass-ceramic materials is decisively important to the success of a large diffraction-limited telescope, and at present little is known about the temporal stability of the candidate mirror substrate materials. This report contains the results of an experimental study of the dimensional stability of glasses and glass ceramics being considered for substrates of massive diffraction-limited mirrors designed for several years of service in earth orbit. The purpose of the study was to measure the relative change in length of the candidate substrate materials, to the order of 5 parts in 10^8, as a function of several years time.

This report treats the development of monolithic test etalons, the development and improvement of two types of ultra-high precision interferometers, and certain aspects of test data presently achieved.

17. KEY WORDS	18. DISTRIBUTION STATEMENT Unclassified — Unlimited *Charles A. Lundquist* Charles A. Lundquist Director, Space Sciences Laboratory

19. SECURITY CLASSIF. (of this report) Unclassified	20. SECURITY CLASSIF. (of this page) Unclassified	21. NO. OF PAGES 48	22. PRICE NTIS

SUMMARY

The purpose of this contract was to determine the temporal stability of four mirror materials relative to Homosil to within 5 parts in 10^8 or 50 ppb. Routine metrology is a part, or so, in 10^6, while aggressive metrology is good to a few parts in 10^7. Clearly this called for an order of magnitude improvement.

To date this contract goal has not been attained. Despite the fact that this is a "final" report, the effort at NBS continues.

Two important components were required for this study. One was an object to measure, and the second was an instrument capable of measuring it to the required precision.

All other stability measurements have involved wringing or contacting "films" and reflective or multiple dielectric coatings. The physical and optical instability of such coatings and films may be large compared to the 10-15 Angstrom precision required. We asserted that our measurement objects would be free of these uncertainties. We also required that the polished (gauging) surfaces of the object be facing the same direction to minimize problems of phase angle upon reflection.

Fortunately, these requirements were satisfied by a monolithic etalon, described later, which had its two gauging surfaces optically polished, flat and parallel. The 26 etalons were produced by the Optical shop at the University of Arizona in Tucson, and it was an impressive

effort on a difficult task.

The other component for this study was the measuring device. This responsibility fell on the metrology experts in the Dimensional Technology department at the National Bureau of Standards.

The report which follows is an excellent account of the development of the polarizing interferometer. It was authored by Dr. Robert J. Hochen and contains the work of many others who contributed to the effort. Near the end of the report are listed the improvements, changes and additions which NBS thinks would allow the interferometer to make length determinations to the required precision. Hopefully, ways and means will be found to accomplish this.

NBS Research Associate Program in Ultra-High Precision Metrology on Behalf of the Corning Glass Works Corning, N. Y.

Robert J. Hochen[*]

I. Introduction

In 1972 the NBS agreed to supervise and administer a Research Associate program in ultra-high precision metrology on behalf of the Corning Glass Works. The objectives of this program were (a) "to develop techniques which will enable consistent dimensional measurements to an accuracy of 5 parts in 10^8; and (b) to validate these techniques by applying them for a statistically significant period of time to materials of known long term dimensional stability".[1][**] As of the date of this report, neither of these objectives has been completely realized, though much has been learned in the attempt. The purpose of this report is to document our efforts so that future workers might profit from our experience.

II. The Experimental Philosophy

Early in this study it was decided that due to budget restrictions absolute length measurements at the part in 10^8 level would not be attempted at NBS. Our approach was instead to compare very similar artifacts (a traditional metrologic approach) in a normal laboratory atmosphere. We hoped in this way to develop techniques better suited for future "routine" metrology and by the use of statistical intercomparison of objects obviate the need for long term interferometer stability.

This approach has much to recommend it. If the objects compared are sufficiently similar all linear correction terms in the length determinations will cancel out in the differences. This includes the normally applied refractive index corrections as well as interferometer and detector instabilities. Furthermore, statistical tests performed on the difference between two "masters" which are included in the measurement algorithm enable the experimenter to monitor process control.[2] Throughout this study artifacts were therefore compared using this so-called "four-one" series algorithm.

III. The Samples

Twenty-six (26) artifacts for use in this study were prepared for NBS by the University of Arizona optical shop, in the geometry shown in Figure 1. This geometry was chosen to (a) eliminate a wringing film by making the platen an integral part of the artifact and (b) to cancel out, in the length measurement, the unknown phase shifts at the reflecting surfaces.
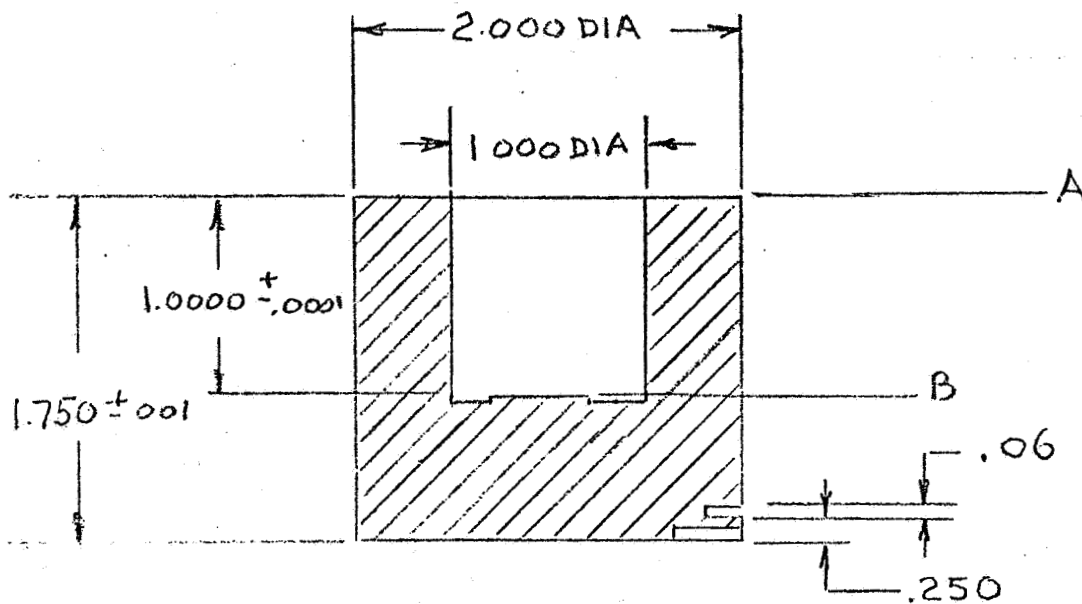

**Figures enclosed in brackets refer to listings under Bibliography at the end of this report

Figure 1: Artifacts for Dimensional Stability Program

½ DIA

½ DIA.

Z — Z

90° V GROOVE
3/8 LG X .092 DP

.187 TYP
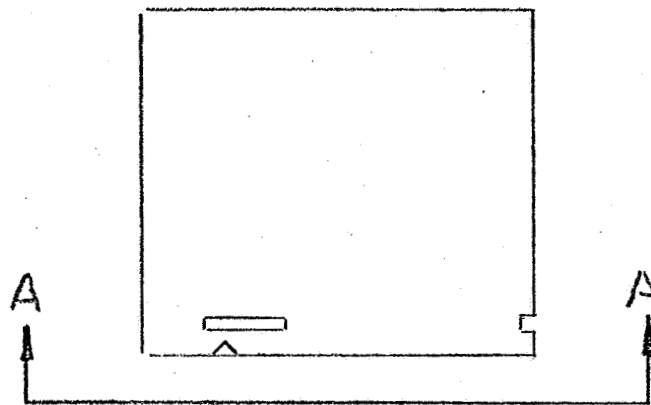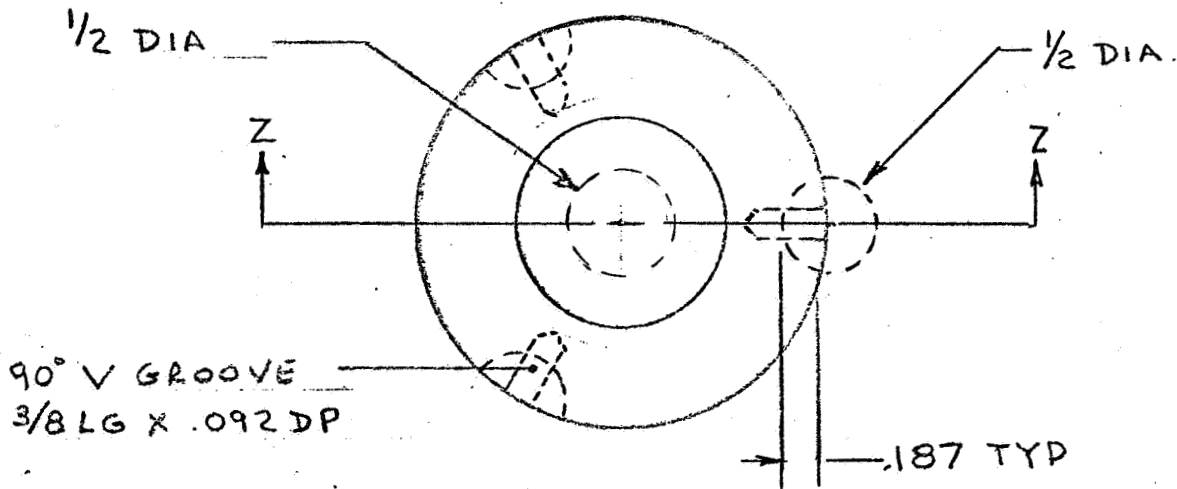
NOTES

1. Surfaces A and B
   flat to $\lambda/10$ per inch

2. Surfaces A and B
   parallel to $\lambda/5$ per inch

A — A

2.000 DIA

1.000 DIA

A

$1.0000 \ {}^{+}_{-} .0001$

B

1.750 ± .001

.06

.250

SECTION Z-Z

These artifacts are identified by a letter-number-letter code. The first letter of the code identifies the material, the number identifies its position in the original block of glass and the last letter indicates whether it came from the top (T) or bottom (B) of the block. An asterisk added at the end of the code meant that the artifact was constructed of two pieces, optically contacted. In Table 1 we list the first letter of the code, the material so designated, and the thermal expansion coefficients as supplied by Corning Glass Works.[3]

Each of the artifacts was checked for parallelism and flatness of the gauging faces. The results of these measurements, performed at NBS and analyzed by Ben Justice at Corning Glass Works (CGW) are given in Table 2. All artifacts used in this study met the design specifications for flatness and parallelism (parallel to $\lambda/5$ per inch, surfaces flat to $\lambda/10$, see Fig. 1).

Except for the last run (AB), all measurements were performed on samples as received from Corning without additional cleaning. The four (4) artifacts measured in the final run (AB) were cleaned following the procedure described in the section on the results of that run. The artifacts were stored, except when being measured, in bell jars supplied by CGW. No attempt was made to control the atmosphere in these containers, since studies at CGW have shown that the surfaces "of SiO_2-TiO_2 glasses should be particularly inert to 'laboratory air' exposure once the 'carbonate' layer is formed".[4]

IV. Mechanical Construction

For all measurements the artifacts were mounted on positioning plates the purpose of which was to insure accurate repositioning of the artifact in the interferometer housing. The goal was to obtain angular repositioning to ± 1 sec. and translational repositioning to $\pm.001$ inch. A schematic of one of these plates is shown in Figure 2 (a) with, and (b) without an artifact in position. The three grooves in the artifact set on three balls located on the set screws in the plate. The artifact is held down by the spring clamps shown in Figure 2b. The flat-groove-cone construction on the plate set against a tripod of balls rigidly attached to the interferometer casing. The flat-groove-cone part of this system worked well, but, for reasons not yet fully understood, the spring clamps, grooves, and balls of the artifact mounting proved unreliable. It is postulated that this was due to breakage of minute pieces of glass in the ground glass grooves. In any case, in order to meet the repositioning specifications, the artifacts were positioned as in the figure, the set screws were adjusted so that the surfaces were perpendicular to the interferometer axis and then the artifact was epoxied to the plate. The artifacts were measured in this mounting configuration for all runs except the last (AB).

For the last run, involving only three of the original 26 artifacts, the mounting was altered slightly. These artifacts were rotated so that

5

Table 1

First Letter of Code	Material	Nominal Linear Expansion Coefficient PPM/°C
C	Cervit 101	−0.034
H	Homosil	+0.492
S	Silica, Corning Code 7940	+0.475
T	Titanium Silicate, Corning Code 7971	−0.035
Z	Zerodur	−0.037

Table 2. Artifact Geometry

Artifact	Parallelism[a]	Flatness[b]
C3T	.01	F
C4T	.03	G
C5T	.01	F
C6T	.01	F
C7B*	.02	VG
C7T	.01	VG
Z3T	.015	G
Z4T	.03	G
Z5T	.03	F
Z6T	.006	F
Z7T	0	G
Z6B*	.01	VG
S7B	.04	P
S7T	.02	F
S8T	.005	P
S9T	.04	F
S11T	.01	F
S11B*	.05	VG
T3B	.04	P
T5B	.05	P
T5T	.03	F
T8T	.09	P
T9B*	.03	VG
T9T	.005	P
H1	.02	G
H2	.016	G

[a] Parallelism here is the average fractional fringe spacing difference between top and bottom surfaces of the artifact.

[b] Estimated flatness of the center bottom, Poor, Fair, Good and Very Good.

7

Figure 2: Positioning Plate

CONE

TRIPOD OF BALLS

FLAT

a)

V-GROOVE

ARTIFACT

b)

SPRING CLIP
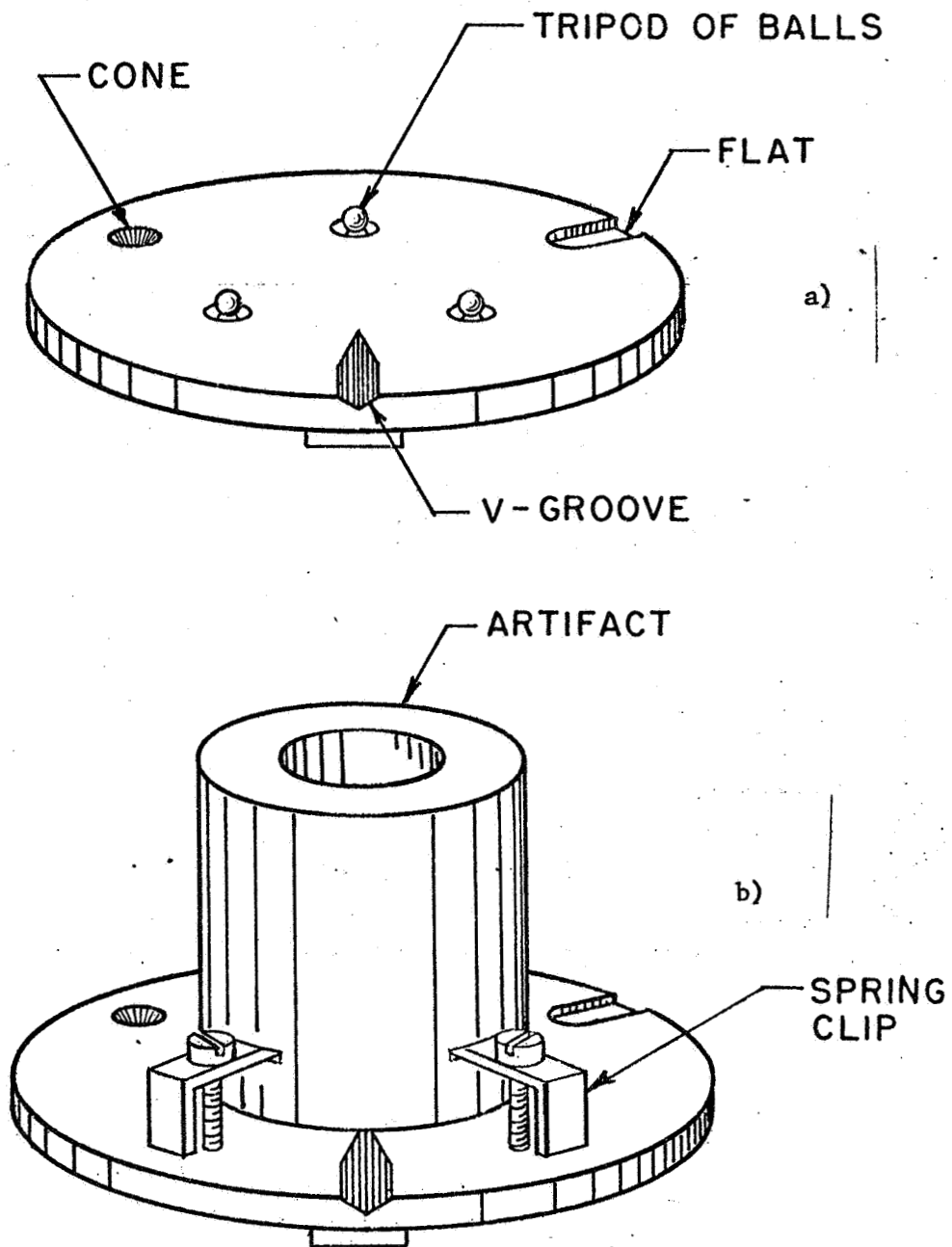
the three balls on the plate were no longer in the grooves, but rested on the relatively smooth bottom surface. Initially one of the balls, the one nearest to the groove, was epoxied to the artifact. The artifact was then adjusted as before. After adjustment all three balls were then epoxied to the plate (but not to the artifact) to prevent translation and rotation of the balls. These artifacts were therefore held on their tripod mount by a combination of a point contact epoxy joint on one ball and the retaining strength of the spring clamps. The artifacts thus mounted also met the design specifications for repositioning accuracy. This mount was adopted in an attempt to mechanically decouple the artifact from the plate and reduce thermal stresses.

In operation, four (4) artifacts were stored on a carousel under the interferometer housing. A mechanical device allowed the operator to remotely position any of the four (4) artifacts on the measurement tripod under the interferometer. This device worked well throughout the experiment. Drawings of it are available upon request.
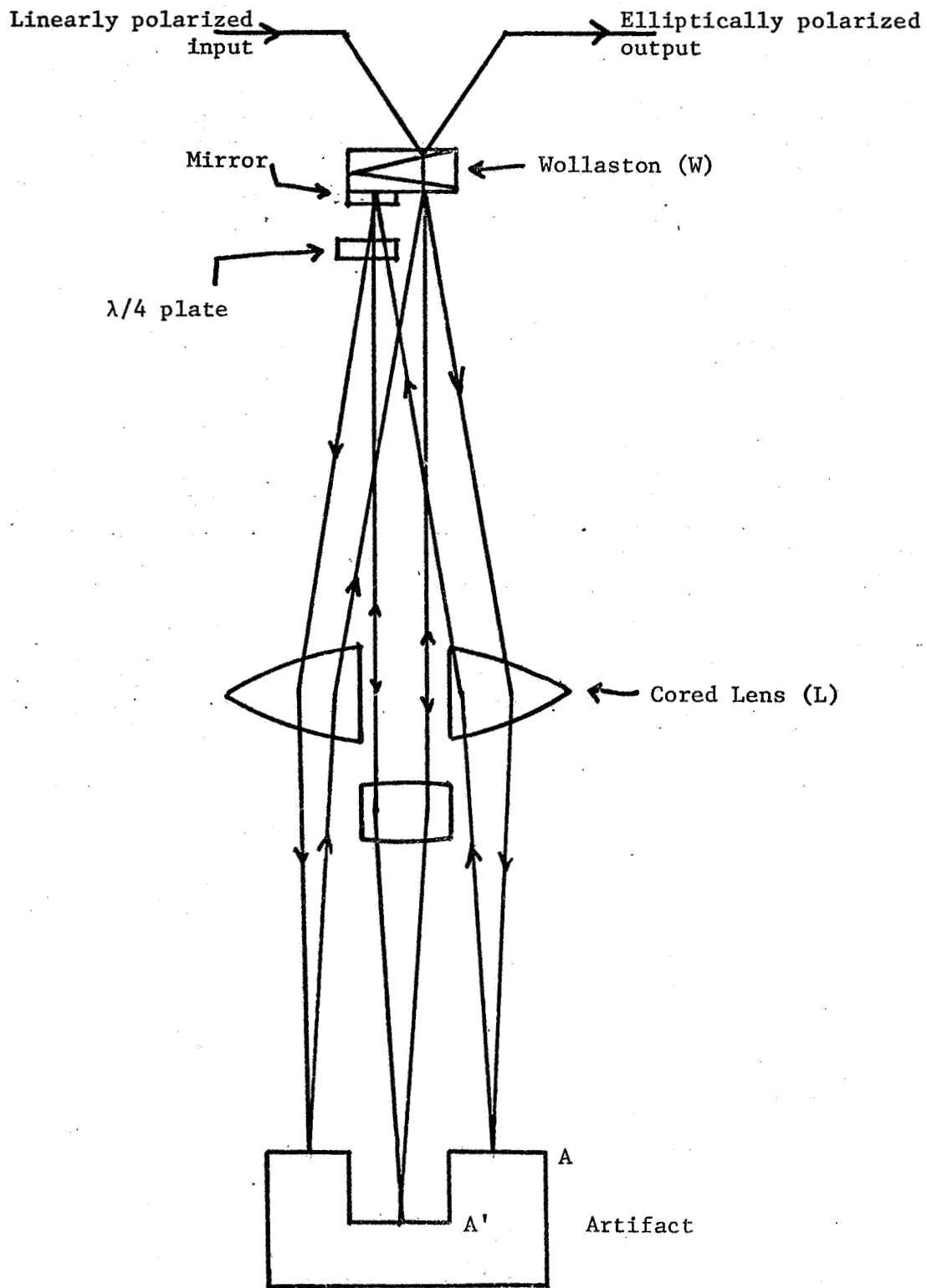
V. The Interferometers

Two interferometers of different geometry were used in this investigation. Both used the same encoding scheme, whereby the phase difference between interfering beams is converted into a polarization angle. Conceptually this process is simple. Two equal amplitude coherent plane waves, left and right circularly polarized respectively, are summed. The angle of polarization of the resulting linearly polarized beam is then proportional to the phase difference between the input beams. In practice the execution of this plan is more complicated, and errors due to imperfections in the optical system can show up in the encoding process. In this section we will describe the geometries of the two interferometers used (so-called "Dyson" and "Hartman-Bennet" interferometers), deferring the discussion of the encoding process to a later section.

(a) The "Dyson" Type Interferometer

The first interferometer used at NBS on this investigation was patterned after an instrument first introduced by Dyson[5]. The NBS instrument was constructed by J. Lazar and A. Hartman. A diagram of this interferometer is shown in Figure 3. The input beam is split into orthogonal polarizations by the compensated Wollaston prism (W). The two polarization states emerge from the prism at different angles. These beams are focused by the cored lens (L) onto the artifact surfaces (A, A'). The reflected beams return through the lens to the silvered portion of the Wollaston (W) passing through a quarter wave plate on the way. The beams are reflected off the Wollaston back through the quarter wave plate. The interior beam travels its original path in reverse, while the exterior beam traverses a path which is the mirror image of its input path. Since the polarizations of the beams have been reversed due

9

Figure 3: Dyson Type Interferometer

Linearly polarized input → ← Elliptically polarized output

Mirror → ← Wollaston (W)

λ/4 plate

← Cored Lens (L)

A

A'   Artifact

to double passage through the quarter wave plate, they are recombined by the Wollaston and exit the interferometer. With proper alignment they may be made colinear and coincident. Another quarter wave plate (not shown) is used to convert these linear orthogonal polarization states to left and right circular polarizations for analysis. Reports have been prepared on the design and behavior of this interferometer and one is included in this report as an appendix. This interferometer was found to be unsuitable for measurement on uncoated artifacts due to difficulties with spurious reflections. For this reason, and because of unexplained large jumps in apparent artifact length, a new interferometer was constructed for use in this investigation.

(b) The "Hartman-Bennet" Interferometer

A schematic diagram of the Hartman-Bennet interferometer is given in Figure 4. The instrument was designed and constructed by A. Hartman in collaboration with S. H. Bennet and J. Lazar. The right two beams (3 and 4) are actually in a plane displaced from the plane of the drawing, with (3) being directly behind (2) when the interferometer is viewed as in the diagram. They are drawn in a plane for ease of explanation.

In this interferometer a plane wave of laser light polarized at 45° to the vertical is incident on the first beam splitter (BS1). The $\vec{s}$ state is reflected by the beam splitting surface and the $\vec{p}$ state transmitted. The reflected $\vec{s}$ state (Beam 1) travels downward through the quarter wave plate, is reflected off the artifact's surface and comes back up through the quarter wave plate. Double passage through the quarter wave plate has rotated the plane of polarization 90° so this beam now passes through the beam splitter (BS 1) enters the cube corner and is redirected downwards through BS 4. It is again reflected off the artifact's surface passing twice through a quarter wave plate. Upon return to BS 4 it is in its original polarization state and is therefore reflected by this beam splitter and passes out of the interferometer. The $\vec{p}$ state which is transmitted by the first beam splitter is converted to an $\vec{s}$ state by a half wave plate and then follows a path similar to that of beam 1 but through beam splitters 2 and 3. After this second beam is reflected off beam splitter 3 it is reconverted to a $\vec{p}$ state by the second half wave plate and thus passes through beam splitter 4 out of the interferometer. As in the Dyson, a separate quarter wave plate (not shown) is used to convert to left and right circular polarizations before analysis.

VI. The Detector

The detector used in this experiment was similar in design to the azimuthal polarimeter of W. B. Olsen.[6] After passage through the final quarter wave plate the light beam, nominally linearly polarized, was directed through a Faraday cell consisting of an ADP crystal centered in a solenoid. This

Figure 4: Schematic of 'Hartman-Bennet' Interferometer

ARTIFACT TO BE MEASURED
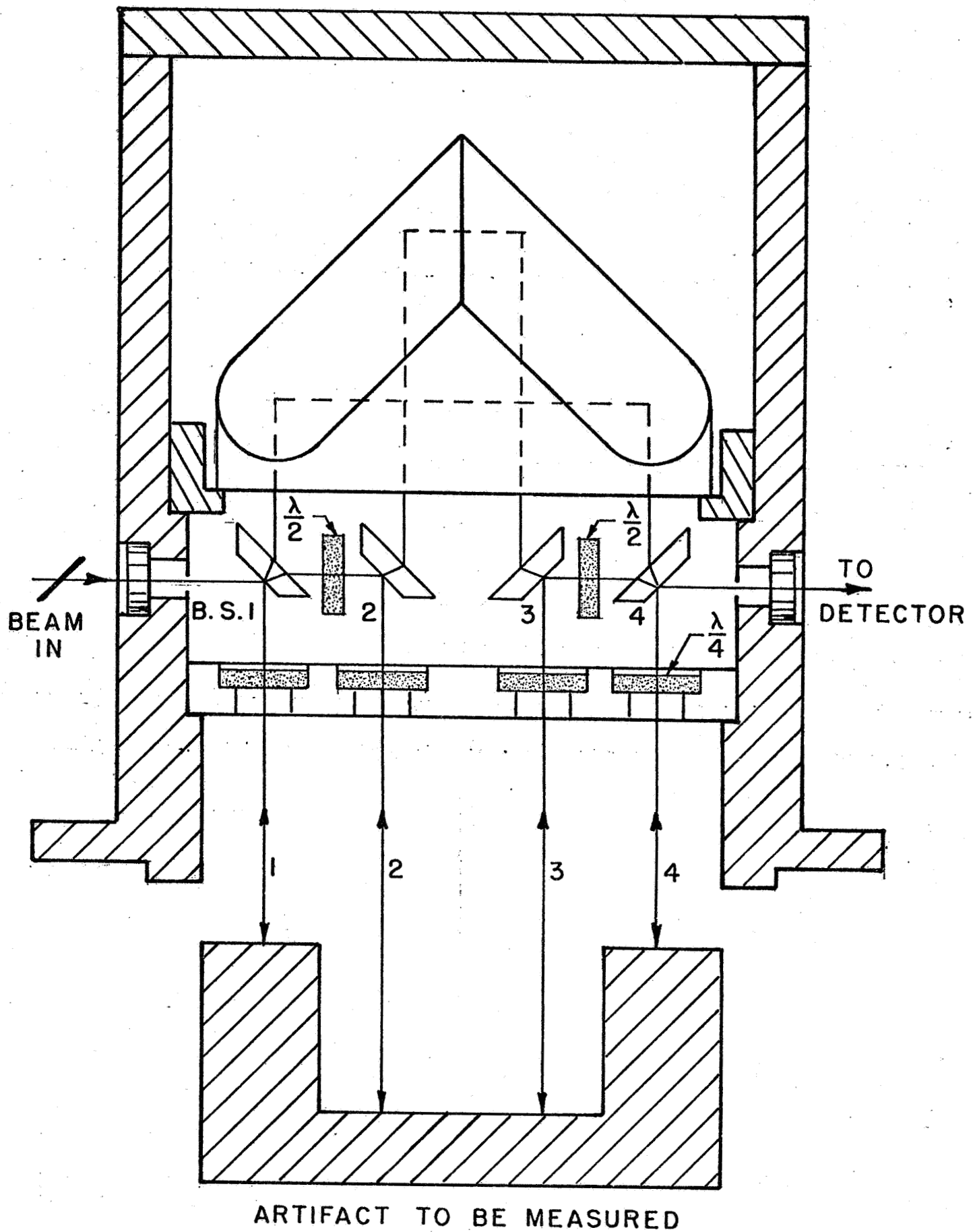
solenoid consisted of copper wire wrapped on a bakelite core. The solenoid was driven with a 200 hertz, 0.5 amp sine wave derived from the output reference of a lock-in amplifier. This cell produced a small modulation ("dither") of the polarization angle of the transmitted beam. The modulated beam then passed through an analyzer, connected to a shaft encoder to sense its position, to a photomultiplier. The ac output of the photomultiplier was returned to the lock-in amplifier through a narrow band filter-amplifier. A detailed analysis of the electrical signal so obtained is given in reference 6 and 7. For our purposes here it suffices to say that when the analyzer was aligned parallel or perpendicular to the plane of polarization of the wave, the in phase output from lock-in goes through zero. This enabled us to set the analyzer on a minima (orthogonal to the polarization plane) to a precision of ±0.1 degrees. A block diagram of this electro-optic system is shown in Figure 5.

VII. Polarization Encoding of Phase Information

The qualitative description of the phase encoding scheme given earlier in this report fails to take into account the nonideality of any optical system. It is, however, these small deviations from ideality which limit the accuracy of interferometers. In this section we will discuss those deviations from ideality we have so far considered and quantify their effects on measurement accuracy. To make the discussion more concrete we present it in reference to a model interferometer in the Michelson configuration (Figure 6). This is about equivalent to one-half (1/2) of the Hartman-Bennet. Rather arbitrarily we divide this model system into three functional blocks: (1) the light source, (2) the interferometer proper and (3) the detector.

Ideally this interferometer operates as follows: A plane wave of fixed frequency ω is emitted from the laser polarized at 45° with respect to the vertical and is incident upon the polarizing beam splitter. Here the beam is split in two equal amplitude waves, in orthogonal polarization states. The $\vec{s}$ state proceeds upon path 1 and the $\vec{p}$ along path 2. Both beams pass through a quarter wave plate, are reflected off a mirror and return to the beam splitter with their polarization states reversed. Beam 1 is therefore transmitted and beam 2 reflected. They emerge from the interferometer colinear and coincident and enter the detector assembly. The metal mirror M_3 simply steers the beam to the quarter wave plate (λ_3) where these $\vec{s}$ and $\vec{p}$ states are converted to left and right circular polarization states. These two states add to yield a wave linearly polarized at an angle dependent upon their relative phase. The Faraday cell-analyzer-photomultiplier assembly operates to detect this angle as described in the detector section of this report.

The above description contains many implicit assumptions. For the source we have examined two of these; the effects of laser frequency changes and the effects of finite beam divergence. For the interferometer we only consider here those effects due to imperfect separation of $\vec{p}$ and $\vec{s}$ states by the beam splitter as the geometric effects are interferometer dependent and are discussed in
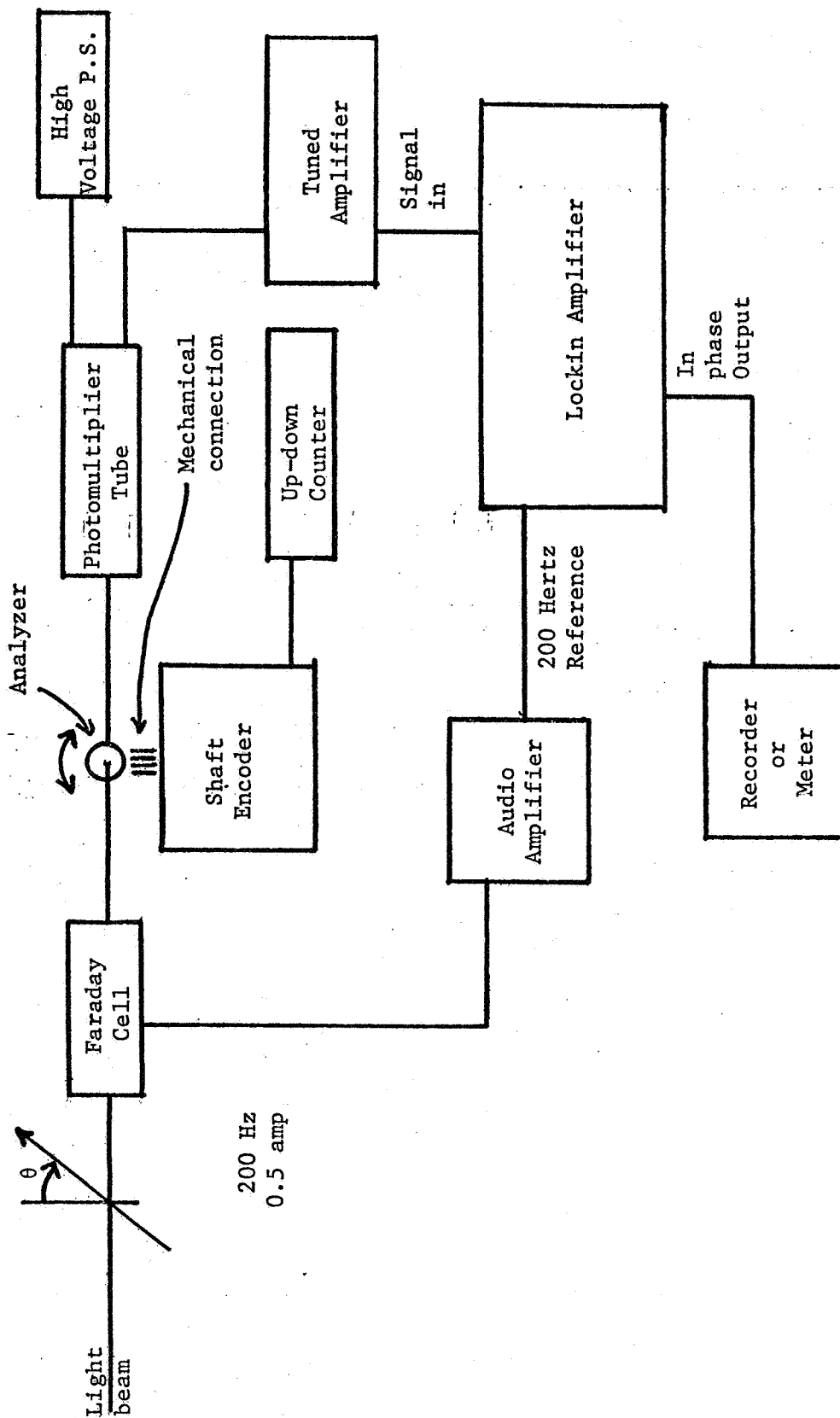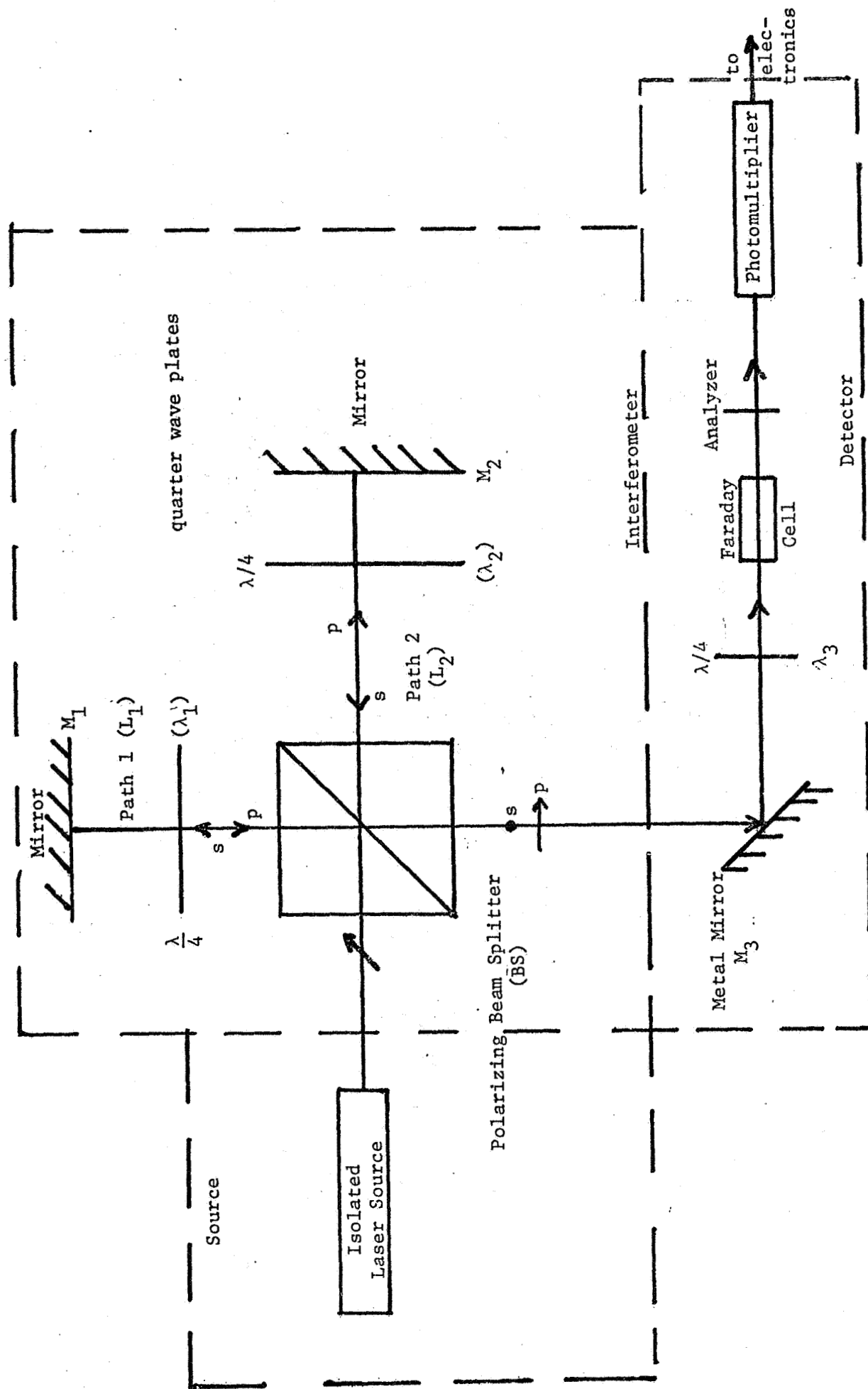
13

Figure 5: The Detector

Figure 6: A Model Polarizing Interferometer (Michelson Configuration)

15

the appendices. In the detector assembly we have looked at the effects due to the metal mirror (M_3), misalignment of the quarter wave plate (λ_3) and imperfect quarter wave plate construction.

The effects of laser frequency on the measurement are trivial to calculate. If $L_1 \neq L_2$ by an amount ΔL then the phase difference between the two beams is just

$$\phi = kn\Delta L. \tag{1}$$

Here ΔL is the total path length difference between the two beams ($k=\omega/c$). If we wish to measure ΔL to a part in 10^8 we must know k to a part in 10^8 (and incidentally n, the refractive index along the unmatched path). In this investigation we compared artifacts of very nearly equal length so that L is effectively a few wavelengths at most (when we take differences) so changes in k ($k = \omega/c$) and n are insignificant. Even so, we used a Lamb dip stabilized laser ($1/10^8$) to avoid this problem.

Phase errors due to beam divergence are also important only if $L_1 \neq L_2$, which is the case in many practical measurement situations. The beam divergence is most easily considered by imagining the beam to be a small portion of a spherical wave front from a very distant source. Let the source be at distance L' from the interferometer assembly (typically α is 3 milliradians for a laser beam and the beam diameter is about 2 mm making $L' \simeq 10^3$ mm). Now let us suppose that the beam continues to diverge at this rate and the paths of the interferometer are unmatched. Then the curvature (phase profile) of the interfering wavefronts will be different at the detector and a circular "bull's eye" type pattern, rather than a single uniform spot, will be seen. The averaging of the detector over such a pattern will depend strongly on edge effects and is difficult to predict.

For a specific idealized example these errors may, however, be estimated. Figure 7 is a schematic drawing of one such simple case. Two wavefronts arrive at the detector surface from virtual point sources ΔL apart. The phase of 1, relative to its phase on axis is just

$$\phi_1 = (\frac{r_1}{\cos \theta_1})k - r_1 k, \tag{2a}$$
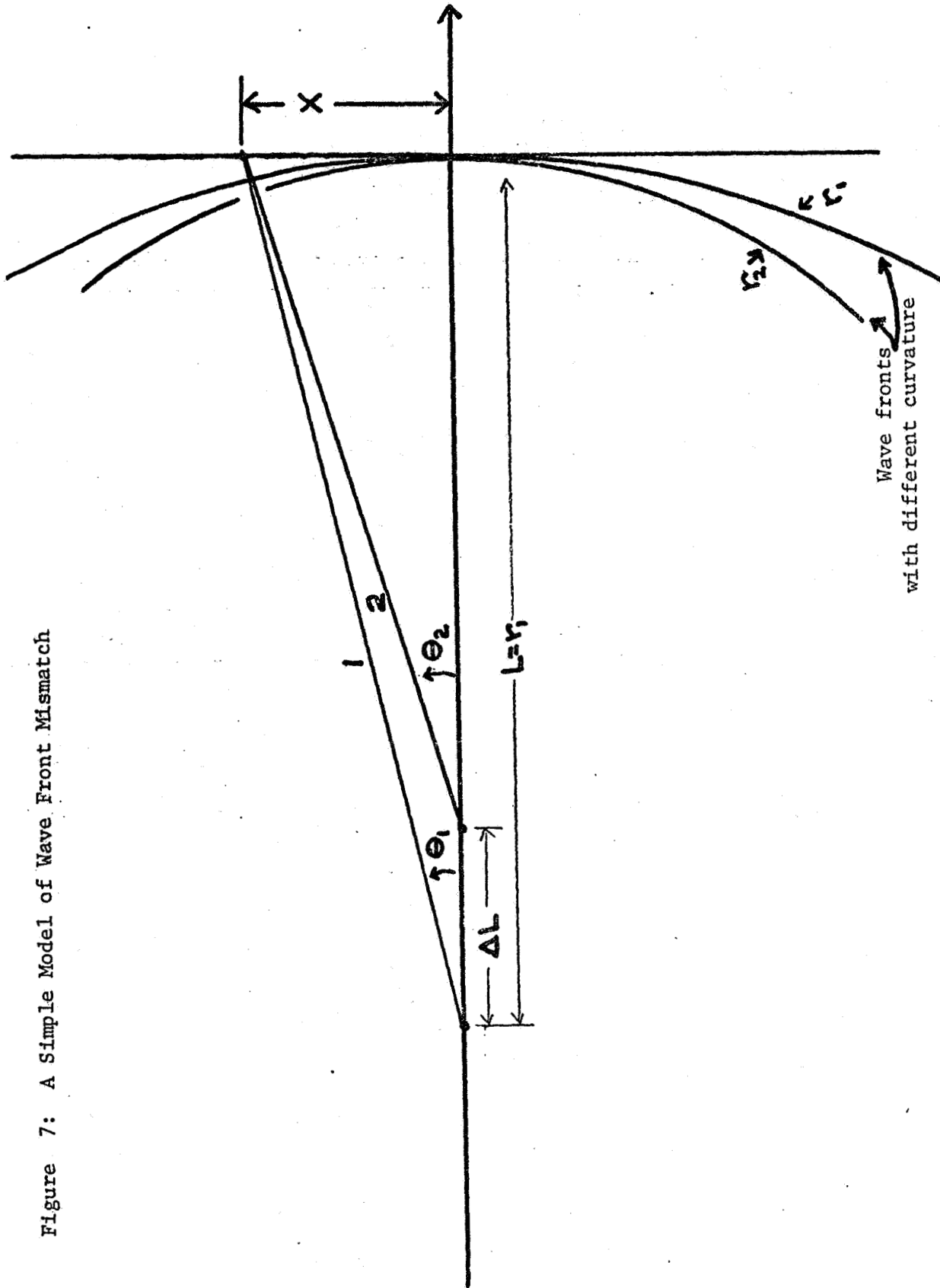
and

$$\phi_2 = (\frac{r_2}{\cos \theta_2})k - r_2 k. \tag{2b}$$

Here the medium is assumed to have refractive index one (1). Letting x represent the off axis distance, radially, the phase difference reduces to

$$\Delta\phi(x) = \phi_1 - \phi_2 = \frac{kx^2}{2} [\frac{\Delta L}{L(L + \Delta L)}], \tag{3}$$

Figure 7: A Simple Model of Wave Front Mismatch

where small angle approximations have been used throughout. If we take x equal to a typical beam radius (.1 cm), $k = 10^5$ cm^{-1}, L = 100 cm and ΔL = 10 cm we find that $\Delta\phi \simeq .5$ radians from the center to the edge of the pattern. In this case an operator would "see" only a single fringe but the phase across this fringe would not be constant.

If this fringe were analyzed with a crossed polarizer the minimum current would not occur when the polarizer axis was 90° with respect to the $\vec{E}$ vector at the pattern center. The output current of the detector will then be given by

$$i \propto \frac{2}{R^2} \int_0^R \cos^2(\theta - \frac{\Delta\phi(x)}{2})\, xdx, \tag{4}$$

where R is the radius of the total pattern. Writing $\frac{\Delta\phi(x)}{2} = \alpha x^2$ (see equation 3) the above becomes

$$i \propto \frac{2}{R^2} \int_0^R \cos^2(\theta - \alpha x^2)\, xdx, \tag{5}$$

which reduces to $i \propto \cos^2\theta$ when $\alpha \to 0$. After integration equation (5) becomes

$$i \propto \frac{1}{2}[1 + (\frac{\sin\beta}{\beta})\cos(2\theta - \beta)], \tag{6}$$

where $\beta = \alpha R^2$. This result also reduces to $\cos^2\theta$ when $\beta \to 0$.

For $\beta < \pi/2$ {the only case we will consider here} the minima will occur when $\cos(2\theta - \beta) = -1$

$$\theta - \beta/2 = \pi/2. \tag{7}$$

since $\beta = \frac{k\Delta L\, R^2}{4L(L + \Delta L)}, = \frac{k}{4}\alpha^2 \frac{\Delta L}{(1 + \frac{\Delta L}{L})}$

It can be seen that the position of the polarizer in order to obtain a minima depends upon the path length difference in a way one might expect intuitively. $\beta/2$ is just the polarization at the radius ($r = R/\sqrt{2}$) where the area inside is equal to the area outside, that is, the "average" polarization of the pattern. In this case above the minimum photo current will be about 2% of the maximum. From the above we conclude that wavefront mismatch will have little effect on results obtained with either the Dyson or Hartman-Bennet interferometers since ΔL is fixed in these systems. In systems where ΔL changes the effect can be large, though, amounting to about 8 mλ/cm with a typical uncollimated He-Ne laser and perhaps be much worse as β exceeded $\pi/2$.

When we consider the effects of the efficiency of the polarizing beam splitter another interesting error emerges. It is possible, if the beam

18

splitter is poor, for some of the $\vec{p}$ state to follow the path intended for the $\vec{s}$ state and vice-versa. We call this phenomena beam mixing. The result will be that the nominally $\vec{p}$ state leaving the interferometer will be the sum of two waves of different phase, one with the intended $\vec{p}$ state phase, and one with the intended $\vec{s}$ state phase. That is

$$E_s = \epsilon_s \epsilon_p E_o e^{i\phi_s} + (1 - \epsilon_s)(1 - \epsilon_p) E_o e^{i\phi_p} \qquad (8)$$

and

$$E_s = \epsilon_s \epsilon_p E_o e^{i\phi_p} + (1 - \epsilon_p)(1 - \epsilon_s) E_o e^{i\phi_s},$$

where the ϵ's are the efficiencies of the beam splitting process. The presence of this effect is easily detected and analyzed. Since the part of the $\vec{p}$ beam on the $\vec{s}$ path will remain in phase with it, the result will simply be to rotate the plane of polarization of the $\vec{s}$ state slightly and vice-versa. One then simply measures the polarization angle difference between the two beams at the output of the beam splitter. If beam mixing is occurring this angle will not be 90°.

The analysis of this effect may be visualized as in Figure 8. For numerical simplicity we set the 'true' $\vec{p}$ state orthogonal to the nominal $\vec{s}$ state. The angle α specifies the nonorthogonality of the two real output polarizations. Call the field in the x direction E_x. It is

$$E_x = E_s e^{i\phi_s} + E_p \sin \alpha \, e^{i\phi_p}$$

and the field in the y direction is

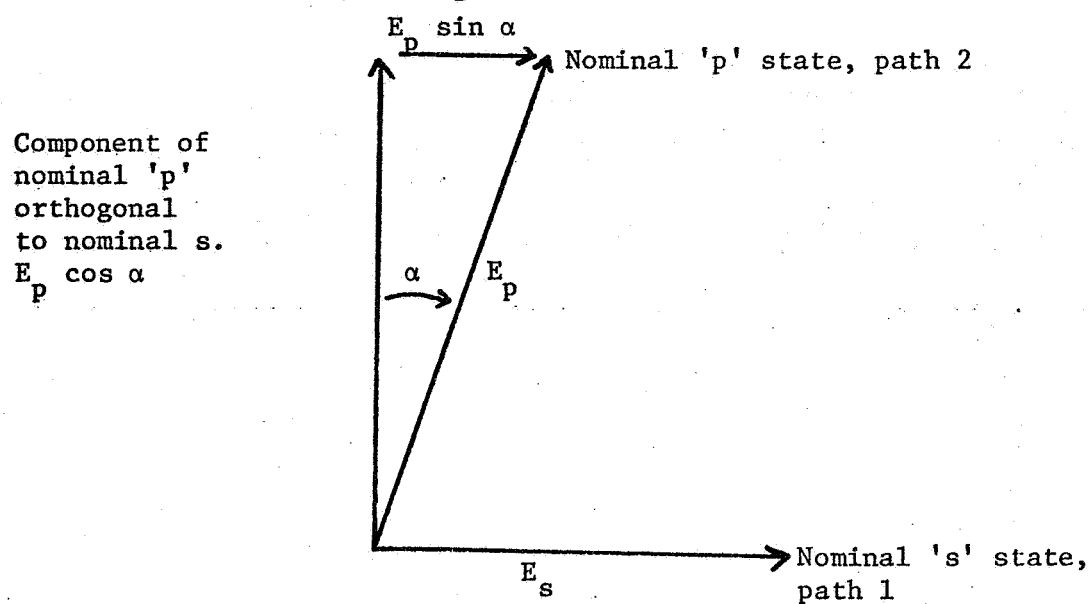$$E_y = E_p \cos \alpha \, e^{i\phi_p}$$

The x field may be easily summed yielding

$$E_x = E e^{i\psi} \text{ where}$$

$$\psi = \tan^{-1}[\frac{\sin \phi_s + \sin \alpha \sin \phi_p}{\cos \phi_s + \sin \alpha \cos \phi_p}]; \qquad (9)$$

and if $E_p \simeq E_s = E_o$, then

$$E = E_o(1 + \sin^2 \alpha)^{1/2} \simeq E_o \text{ for small } \alpha.$$

19

Figure 8: Polarization vectors in a system with
           beam mixing

Component of
nominal 'p'
orthogonal
to nominal s.
$E_p \cos \alpha$

$E_p \sin \alpha$

Nominal 'p' state, path 2

α

E_p

E_s

Nominal 's' state,
path 1

We may arbitrarily choose $\phi_p = 0$ which makes

$$\psi = \tan^{-1}[\frac{\sin \phi_s}{\cos \phi_s + \sin \alpha}]. \tag{10}$$

We assume out detector senses the phase difference between the x and y components of the electric field and therefore measures ψ, which except when $\alpha = 0$, is not equal to ϕ_s, the quantity we want to measure. Plotted in Figure 9 is an error curve with $\alpha = 3°$ (.05 radians) a typical nonorthogonality observed for artifact H1 in the Hartman-Bennet interferometer. Plotted is the difference $\psi - \phi_s$ versus ϕ_s. As may be seen the error depends on ϕ_s (which in our setup was in turn changing due to pressure and temperature fluctuations) in a nonlinear fashion, and when ψ differences are taken between artifacts with different ϕ's, errors can have any magnitude up to twice the extrema of the curve and of either sign.

After the beams leave the interferometer they are incident on the plane metal mirror at angle θ_1. $\vec{s}$ and $\vec{p}$ are now orthogonal. The simplest case is when $\vec{p}$ is in the plane of incidence ($||$) and $\vec{s}$ is perpendicular ($|$) to the plane of incidence. See Figure 10a. In that case they are merely phase shifted a different amount[8] with

$$\Delta\phi_s' = \frac{2vn_1 \cos \theta_1}{v^2 + u^2 - n_1^2 \cos^2 \theta_1}, \tag{11}$$

$$\Delta\phi_p = 2n_1 n_2^2 \cos \theta_1 \left(\frac{2k_2^1 u - (1 - k_2^2)v}{n_2^4(1 - k_2^2)^2 \cos^2 \theta_1 - n_1^2(v^2 - u^2)} \right), \tag{12}$$

where

n_1 = refractive index of air

n_2 = refractive index of metal

$k_2 = (\lambda/4\pi) \chi_2$ where χ_2 is the adsorbtion coefficient of the metal.

The quantities u and v are defined by nonlinear equations with

$$u^2 - v^2 = n_2^2(1 - k_2^2) - n_1^2 \sin^2 \theta_1, \tag{13a}$$

$$vu = n_2^2 k_2^2. \tag{13b}$$

21

Figure 9: Errors due to Beam Mixing

$\alpha = 3°$

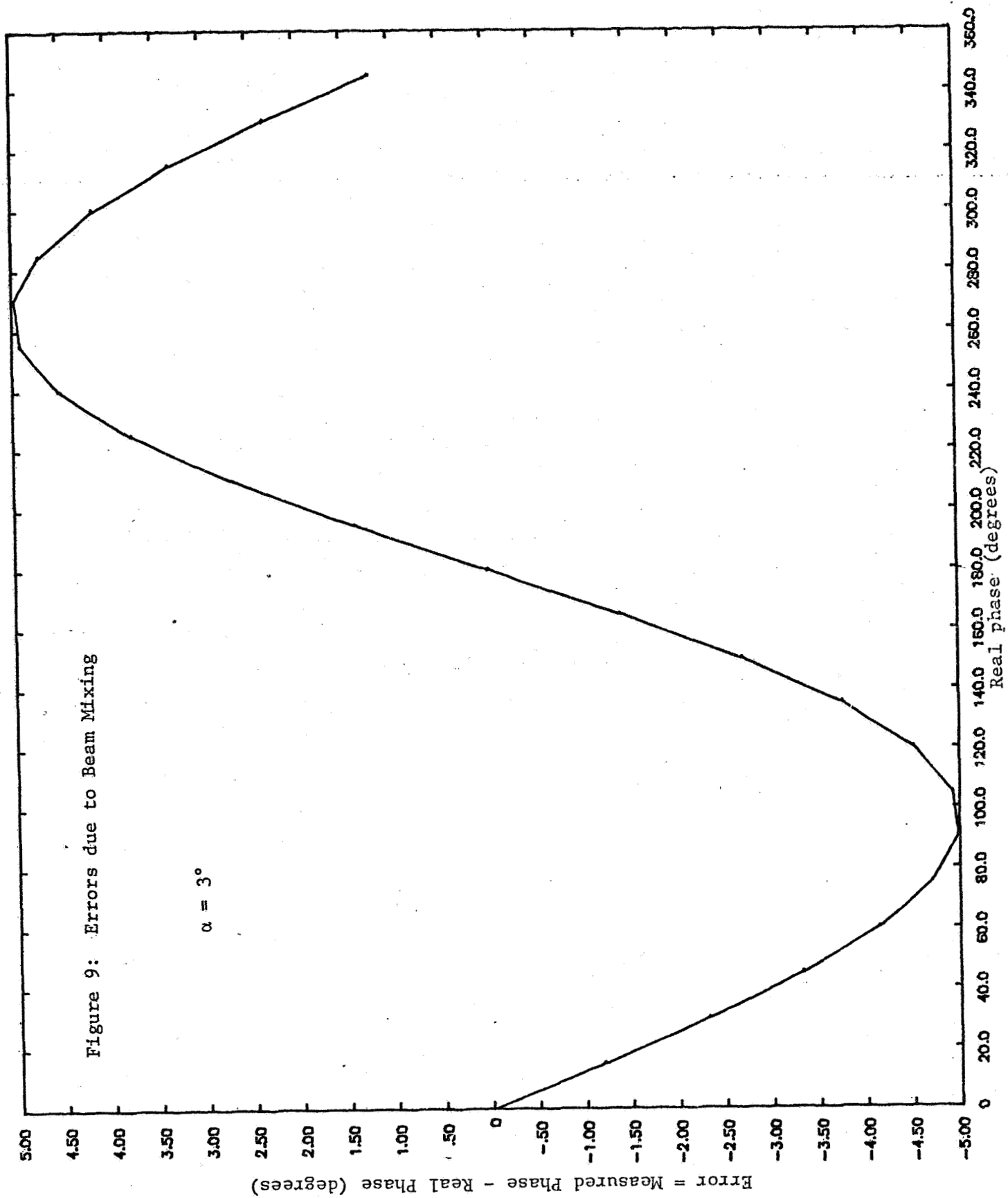Error = Measured Phase − Real Phase (degrees)

Real phase (degrees)

22

Figure 10a: Reflection from a metal surface. $\vec{p}$ in plane of incidence.

$\hat{n}$ – normal to surface

Input beam

$\vec{p}$

$\vec{s}$

θ_1
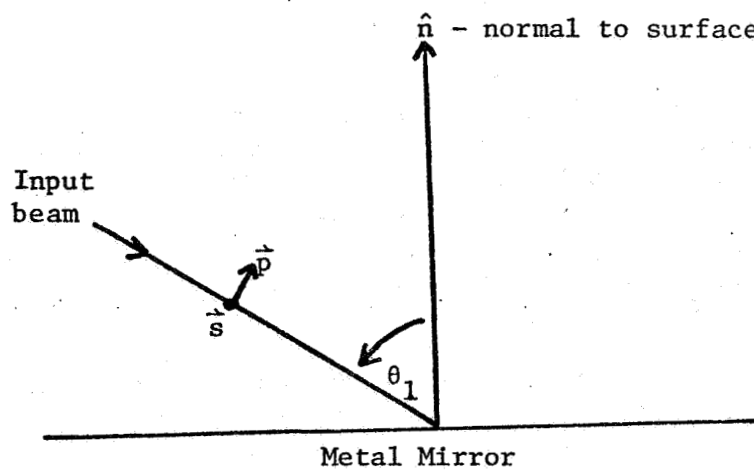
Metal Mirror

Figure 10b: Reflection from metal surface. $\vec{p}$ not in plane of incidence.

$\hat{n}$ = normal to surface

Plane of incidence

Input beam

$\vec{p}$

$\vec{s}$

θ_1
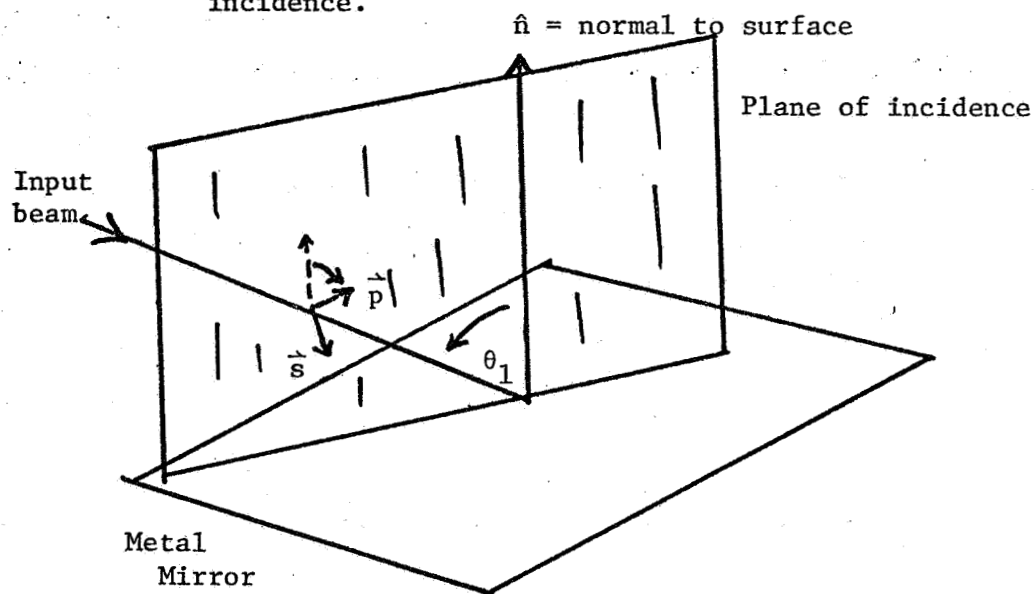
Metal Mirror

Both phase changes are strongly dependent on the metal's properties, the refractive index of the air, and the angle of incidence. Since metal mirrors are known to oxidize, one must expect that for long-term absolute measurements, surfaces of this type should be avoided so that $\Delta\phi_s - \Delta\phi_p$ will be independent of time. For difference measurements the simple effect outlined above should cancel out except for minute changes in θ_1 between artifacts.

Now let us rotate the mirror slightly so that $\vec{p}$ is no longer parallel to the plane of incidence. ($\vec{s}$ will now no longer be perpendicular to this plane either.) This likely approximates a real experimental situation, since perfect mirror alignment would be fortuitous indeed. Now both $\vec{p}$ and $\vec{s}$ have components $\parallel$ and $\perp$ to the plane of incidence and both waves are reflected with elliptical polarization. In the case of the $\vec{p}$ state the major axis of this polarization will be $\parallel$ to the plane of incidence; the major axis of the $\vec{s}$ state will be $\perp$. Let γ be the angle that these states make with the plane of incidence, where γ is assumed to be fairly small (7° or less) so the ellipticity of the resulting light will not be visually apparent (Figure 10b).

Let us call the two phase shifts $\phi_{\parallel}$ and $\phi_{\perp}$ and switch to the reference system defined by the mirror. Then the resulting fields are

$$E_{\parallel} = E_p \cos\gamma \; e^{i(\phi_p + \phi_{\parallel})} + E_s \sin\gamma \; e^{i(\phi_s + \phi_{\parallel})}$$

and   (14)

$$E_{\perp} = E_s \cos\gamma \; e^{i(\phi_s + \phi_{\perp})} - E_p \sin\gamma \; e^{i(\phi_p + \phi_{\perp})}$$

We can only assume that our detector again analyzes the phase difference between the two perpendicularly polarized waves ($E_{\parallel}$ and $E_{\perp}$). That is, a metal mirror in the system might produce "beam mixing" such as discussed in the preceding paragraphs since a simple rotation will not unmix the terms in 14. If $E_p \simeq E_s \simeq E$ then

$$E_{\parallel} \simeq E \; e^{i\psi_{\parallel}}, \text{ with}$$

$$\psi_{\parallel} = \tan^{-1}\left[\frac{\sin(\phi_p + \phi_{\perp}) + \sin\gamma \; \sin(\phi_s + \phi_{\parallel})}{\cos(\phi_p + \phi_{\parallel}) + \sin\gamma \; \cos(\phi_s + \phi_{\parallel})}\right];$$

and $E_{\perp} \simeq E \; e^{i\psi_{\perp}}$, where   (15)

$$\psi_{\perp} = \tan^{-1}\left[\frac{\sin(\phi_s + \phi_{\perp}) - \sin\gamma \; \sin(\phi_p + \phi_{\perp})}{\cos(\phi_s + \phi_{\perp}) - \sin\gamma \; \cos(\phi_p + \phi_{\perp})}\right].$$

We will not carry this analysis any further numerically, but content our-
selves with the comment that at the 1/100 fringe level such "beam mixing"
terms are highly undesirable as evidenced in Figure 9. In both the "Dyson"
and "Hartman-Bennet" interferometers two aluminum coated mirrors (exact
orientation unknown) were used to steer the interfering beams into the
quarter wave plate - polarization detector assembly on all runs except AB.
It would appear from the above that this seemingly innocent design feature
adds a complication that would be best eliminated.

We now will examine the efficacy of the polarization-phase detector
when the quarter wave plate is perfect, but imperfectly aligned. In Fig-
ure 11 we depict this situation, where the axes of the quarter wave plate
are the x and y axes. We use ε to denote the angle out of alignment. The
output fields from beams 1 and 2 are then

$$\vec{E}_1 = A_1 \cos(\pi/4 - \varepsilon) \cos \omega t \ \hat{i} + A_1 \sin(\pi/4 - \varepsilon) \cos(\omega t - \pi/2) \ \hat{j}, \tag{16a}$$

$$\vec{E}_2 = A_2 \cos(\pi/4 + \varepsilon) \cos (\omega t + \phi) \ \hat{i} - A_2 \sin(\pi/4 + \varepsilon) \cos(\omega t + \phi - \pi/2) \ \hat{j}, \tag{16b}$$

where A_1 and A_2 are the incident amplitudes.

With $A_1 \neq A_2$ and $\varepsilon \neq 0$ the resultant of these two fields will not be
linearly polarized but rather elliptically polarized. This will cause no
detection problems as long as the major axes of the ellipse remain along
the axis determined in the ideal ($A_1 = A_2$, $\varepsilon = 0$) limit.

To test this we will assume ε to be small ($\varepsilon < 5°$), and the amplitude
ratio $A_2/A_1 \equiv \delta$ to be near unity. The fields, defined on the quarter wave
plate axes are then, except for constant amplitude factors,

$$E_x = (1 + \varepsilon) \cos \omega t + \delta(1 - \varepsilon) \cos(\omega t + \phi), \tag{17a}$$

and

$$E_y = (1 - \varepsilon) \sin \omega t - \delta(1 + \varepsilon) \sin(\omega t + \phi). \tag{17b}$$

By replacing ωt by θ we can see that these equations describe an ellipti-
cally shaped figure as a function of θ. The amplitude of this figure is

$$R = (E_x^2 + E_y^2)^{1/2} = (x^2 + y^2)^{1/2}$$

which will have extrema at $\frac{dR}{d\theta} = 0$. Since R has no zeros in the domain of
interest this condition for extrema can be rephrased as

Figure 11

quarter
wave plate
axes

$\hat{j}$

$\pi/4$

s-state (Beam 2)

ε

$\hat{i}$ Fast axis

p-state (Beam 1)
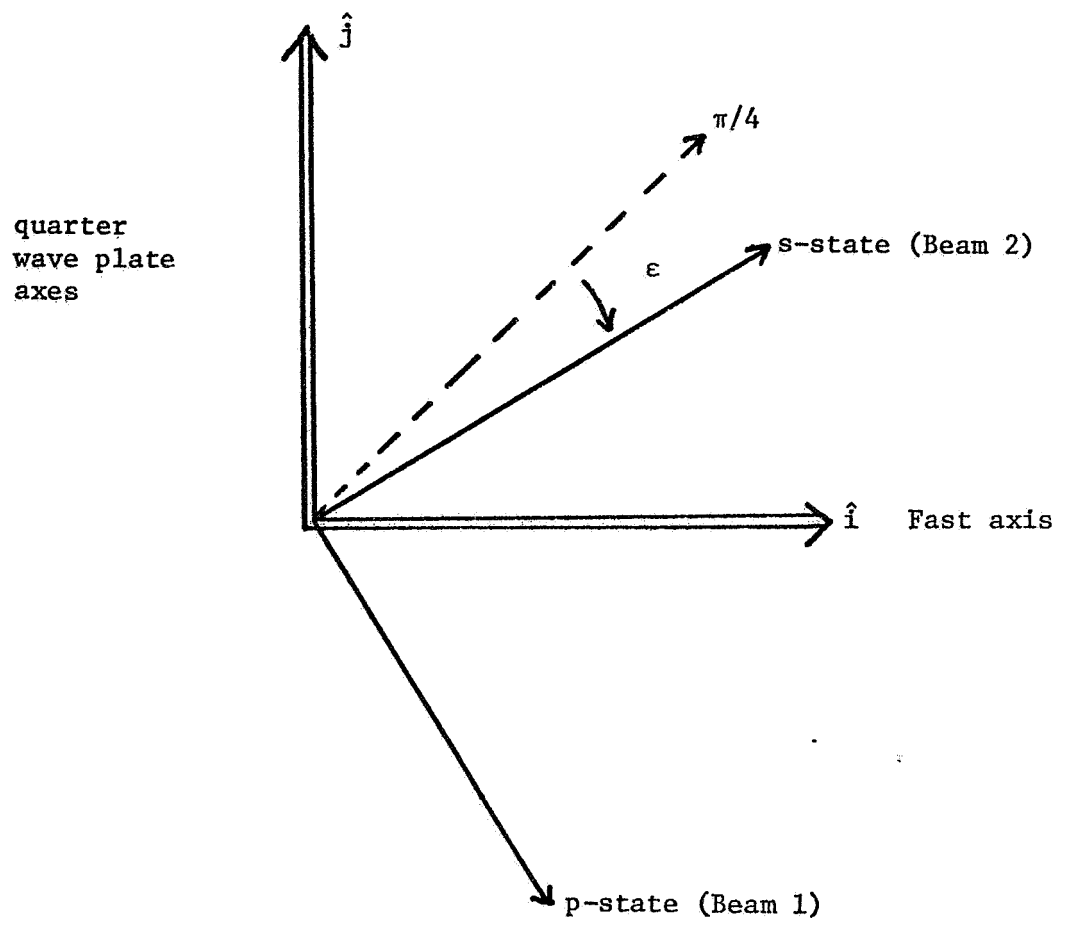
$$x \frac{dx}{d\theta} + y \frac{dy}{d\theta} = 0 \ . \tag{18a}$$

After manipulation of the equation the condition may be expressed as

$$-4\varepsilon \cos \theta \sin \theta + 4\varepsilon\delta^2 \sin(\theta + \phi) \cos(\theta + \phi) - 2\delta(1 + \varepsilon^2) \sin(2\theta + \phi) = 0 \tag{19}$$

The roots of 19 can be readily seen to occur at $\theta = -\phi/2$ for $\varepsilon = 0$. If we assume that perturbations of these roots due to finite ε are small, Equation 19 can be solved. Assuming that $\theta = -\phi/2 + \beta$ yields

$$\beta \simeq \frac{(\delta^2 + 1) \ \varepsilon \ \sin \ \phi}{2\delta(1 + \varepsilon^2) - 2(\delta^2 - 1) \ \varepsilon \ \cos(\phi)}, \tag{20}$$

where we have neglected terms quadratic in β.

Equation 20 indicates that encoding errors due to final quarter wave plate misalignment are of the worst type imaginable. Not only do they depend upon the misalignment angle and the amplitude ratio but also upon the input phase difference in a nonlinear way.

If the detector quarter wave plate is fairly well aligned (ε small) and δ is near 1, the error predicted by 20 closely resembles a sine wave of argument ϕ and amplitude ε.

We now will assume that the quarter wave plate is perfectly aligned but imperfectly constructed. That is the phase shift introduced is not $-\pi/2$ but $-\pi/2 + \varepsilon$ where ε is small. If we let the amplitudes of the input states be equal we find (using the notation of the previous discussion)

$$E_x \propto \cos \theta + \cos(\theta + \phi)$$

$$E_y \propto \sin(\theta + \varepsilon) - \sin(\theta + \varepsilon + \phi) \tag{21}$$

Solving equation $\quad E_x \dfrac{dE_x}{d\theta} + E_y \dfrac{dE_y}{d\theta}$ for its zeros we obtain:

$$\varepsilon[\cos 2\theta - \cos(2\theta + \phi) + \cos(2\theta + 2\phi)] - 2 \sin (2\theta + \phi) = 0, \ \cdot$$

where terms quadratic in ε have been omitted. For $\varepsilon = 0$ the above gives the zero at $-\phi/2$ as expected. When $\varepsilon \neq 0$ we expect the perturbation on the zeros to be small. Substituting $\theta = -\phi/2 + \beta$ and solving to first order in β yields

$$\beta = \varepsilon[\frac{2 \ \cos \ \phi-1}{4}], \tag{22}$$

another small sinusoidal phase dependent error term. Even for the best quarter wave plates currently manufactured ϵ can be of the order of a few degrees, which since $|\beta|_{max} = 3\ \epsilon/4$ means an error of nearly the same magnitude in the observed phase. It should also be noted that ϵ is also temperature dependent and therefore Equation 22 also introduces unwanted temperature coefficients.

It seems clear from the preceding discussion that at the level of $\lambda/100$ (about two degrees of phase shift) there are many barriers that prevent proper functioning of even the most carefully constructed polarization interferometer. Mode matching (wavefront matching) will be a must if large errors in the correct fringe fraction are to be avoided in absolute measurements. More importantly even in difference measurements there are non vanishing, phase dependent terms from "beam mixing" (non-orthogonality of the output polarization states), metal surface reflections in the wrong place, quarter wave plate alignment, and quarter wave plate construction. The nature of these errors are such that they only distort the output as a function of ϕ when interpolations between zeros are attempted. In other words fringe counting with a polarization interferometer would be quite feasible and distortions between zero crossings would be of the form of harmonics of quite small amplitude. Obviously such distortions would be quite difficult, if not impossible, to detect by observation of the detector output as a function of ϕ.

Some of the above errors could be readily removed now that they have been recognized. Beam mixing is the most obvious of these. The detector errors, on the other hand, appear more difficult to eliminate given present quarter wave plate construction and conventional alignment procedures. The methodology of detection will have to be carefully reconsidered in future polarization interferometers.

It is perhaps fortunate that it was decided to conduct these measurements in air rather than vacuum. Had they been performed in vacuum the phase difference between interfering beams would have been nearly constant for each artifact and phase dependent systematic errors probably not discovered. The apparent precision of the measurement would have been much improved and the real accuracy possibly never assessed.

VIII. The Data

After an initial testing period in which the mechanical and optical elements of the system were studied it was decided to attempt dimensional measurements even though some aspects of the system were not in control. We report here the results from four runs labeled for reference purposes runs T, U, AA and AB. The first three of these runs (T, U, and AA) are comparable since they made measurements on the same artifacts in the same system. Run AB was designed to test for, and possibly eliminate, the

effects of thermal stresses and cleanliness and thus should be considered a separate experiment. For this run the artifacts were mounted differently and were thoroughly cleaned.

In Figure 12 we plot the length difference between the two artifacts H1 and H2 which were included in all three runs (T, U, and AA) as a function of time. Except for the conversion to microinches this is raw data. Shown on one of the points is the average uncertainty in each data point obtained from process precision at the time of measurement. It was clear from these results that the process was not in control, and further analysis was necessary.

Since run AA was the best characterized, most recent, and most tightly grouped in Figure 12 we chose to study this data in detail and apply what we learned to the other data, rather than attempt to analyze it all together.

Run AA, begun 6/15/75 and ended 7/29/75, consisted of 32 sets of measurements of four artifacts. Only H2 and H1 were present throughout the whole run. The other two artifacts in any measurement were selected from the remaining 26, each group of two being measured at least four (4) times. Since H1 and H2 were the best determined we concentrated our data analysis attempts on the difference δ_{12} (length of H1 - length of H2).

This difference was examined for temperature, pressure, humidity, and temporal dependence. An anomously large temperature coefficient was found in these data, but there was no statistically significant linear dependence on pressure, humidity, or time. The temperature coefficient difference (run AA) was found to be about 2.1 ppm/deg. C. When we use this value to correct all data to 20 °C the difference δ_{12} appears to be in better control. The corrected differences are plotted versus time in Figure 13. This figure should be compared to Figure 12 where the uncorrected data are plotted.

The data from run AA were next analyzed for nonlinear terms due to beam mixing as discussed in Section VII. Plotted in Figure 14 is the measured phase difference $\Delta\psi_{12}$ between artifacts H1 and H2 versus the phase of one, ψ_1, after corrections for the known temperature coefficient.

The skewed parabola, characteristic of beam mixing errors (see Figure 9), appears as expected since the output beams were nonorthogonal by approximately 4 degrees. These data were then fitted to an equation of the form:

$$\Delta\psi_i^{12} = \frac{1}{2}\left[\tan^{-1}\left[\frac{\sin(\phi_i^1)}{\cos\phi_i^1 + \sin\epsilon_1}\right] - \tan^{-1}\left[\frac{\sin\phi_i^2}{\cos\phi_i^2 + \sin\epsilon_2}\right]\right] + B(T_i - \overline{T}), \qquad (23)$$

Figure 12: Raw Data Runs T, U, AA

Run AA
Run U
Run T

Time (Arbitrary Units)

δ_{12} (μinches)
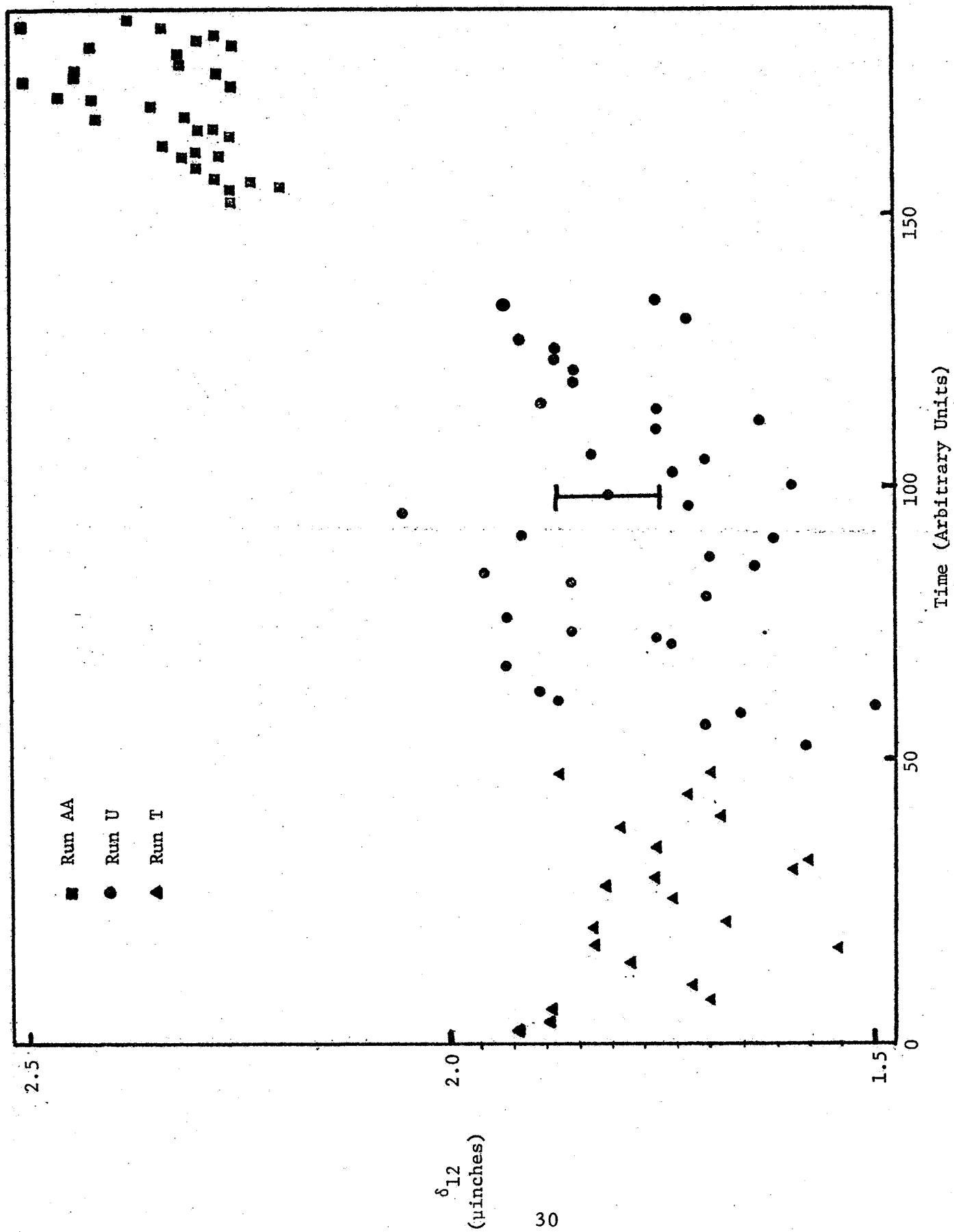
2.5

2.0

1.5

0

50

100

150

30

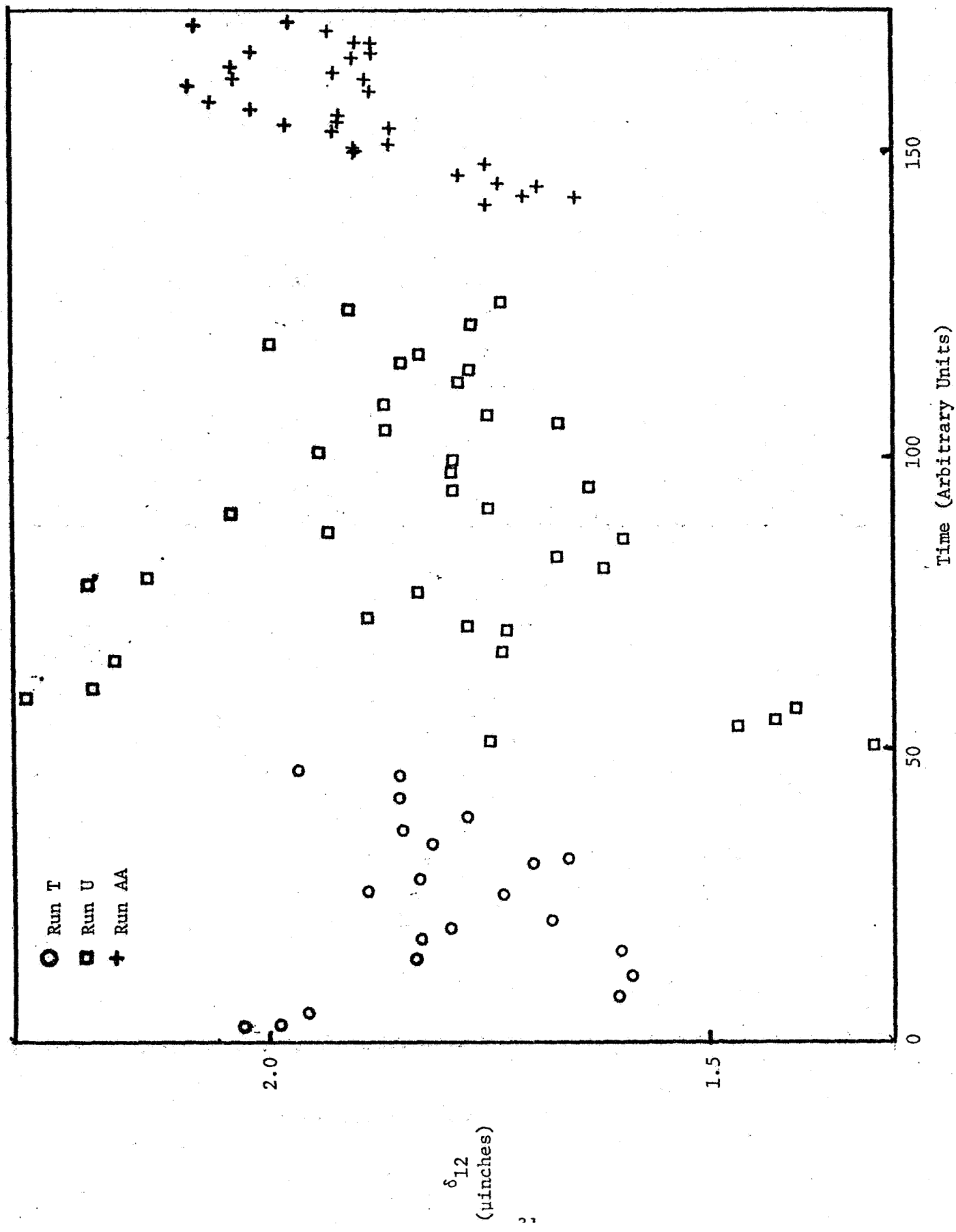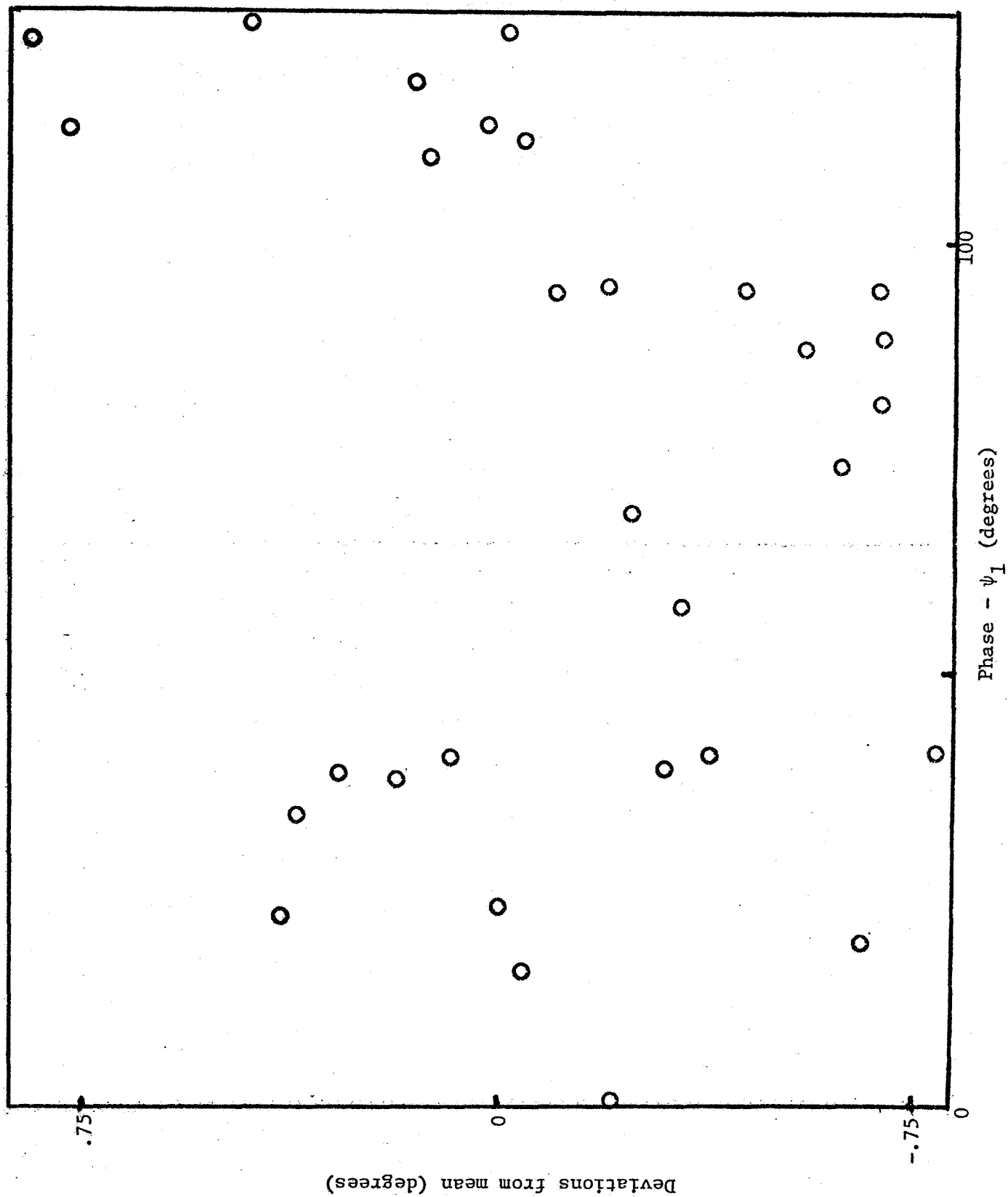Figure 13: Data-corrected to 20 °C using statistically generated temperature coefficient.

Figure 14: Deviations from mean for δ_{12}. Run AA data after temperature correct.

(1 deg. $\approx$ .034 microinch)

Phase – ψ_1 (degrees)

Deviations from mean (degrees)

32

where $\phi_i{}^1 = C_1 - 2\,\psi_i{}^1$

$$\phi_i{}^2 = C_1 - 2\,\psi_i{}^1 + C_2 = \phi_i{}^1 + C_2$$

$$\bar{T} = \sum_{i=1}^{N} T_i/N.$$

C_1, C_2, ε_1 and B were adjustable parameters. The fit gave a reduced chi-squared, $\chi_v{}^2 = 1.36$, with N = 30 points. The best fit parameters were:

$$B = -63.7 \pm 8 \text{ deg.(analyzer angle)/deg. C}$$

$$\varepsilon_1 = 5.6 \pm 0.8 \text{ degrees}$$

$$C_1 = 0 \pm 4 \text{ degrees}$$

and $\qquad C_2 = 138.0 \pm .5$ degrees (phase).

The $\chi_v{}^2$ for the same data set was 2.97 before the "double tangent" beam mixing correction curve was added to the fit. The error in the phase difference (C_2) amounts to a length error of .009 μin., i.e. better than 1 part in 10^8 on the 1 inch artifacts.

A deviation plot from this fit, however, is still not normally distributed indicating residual errors. The source of these residuals could easily be any one or all of the other uncontrolled variables discussed in the previous sections.

It was also discovered in this run (AA) that the nonorthogonality of the output polarization states was not independent of the artifact being measured. Our inability to explain this effect, the inexplicable large temperature coefficient, and the lack of knowledge of quarter wave plate and mirror alignment precluded any more sophisticated analysis of these data.

An attempt was made to analyze runs T and U in conjunction with AA using the double tangent formula. Since no attempt had been made to keep track of the phase on the older runs we estimated it from the pressure. This attempt was unsuccessful possibly due to the phase estimate but more likely due to the larger (unexplained) scatter on the older runs.

The presence of the anomalously high temperature coefficient and the beam mixing term in the length difference between our two "masters" (H1

and H2) precludes any valid measurement of the other artifacts. There are simply insufficient data to determine with any statistical signifi- cance the relevant temperature coefficients and beam mixing terms in these measurements.

In order to try to eliminate some of the problems discovered in run AA, a second run AB was begun on 11/6/75. Many details of this run differed sig- nificantly from those in previous runs. Only four artifacts were measured. This set included three artifacts from the previously measured group (H2, C4T, and Z7T) along with a two inch quartz optical flat (F1) with a good long term history. This flat was flat to $\lambda/10$ and had been measured as long ago as 1967. It was included in the series to separate interferometer temperature coefficients from artifact coefficients. These four artifacts were all cleaned and mounted in the following manner. First they were immersed for 1/2 hour in an ultrasonic bath filled with near boiling water and a standard lab detergent. They were then removed, rinsed in distilled water and blown dry with water pumped super dry Nitrogen (99.5% Assay). They were then immersed in near boiling distilled water, and again subjected to ultra- sonic for 1/2 hour. They were dried as previously. For the final cleaning they received a 1/2 hour ultrasonic bath in boiling ACS methanol. They were quickly blown dry with Nitrogen and stored in laboratory air in a sealed bell jar supplied by CGW. The bell jar had been rinsed in methanol and blown dry with Nitrogen to remove residual oils and dust from it be- fore storage.

These artifacts were then mounted on refinished mounting plates chosen from those used previously. The mounting procedure was designed to mech- anically decouple the artifacts from the plates and is described in the latter part of Section IV.

These artifact-plate assemblies were then placed in the interferometer and aligned so the gauging surfaces were perpendicular to the interferometers optic axis to within $\pm$ 2 sec. During this process it was discovered that the alignment of the etalons in the previous runs had been off several minutes due to a computational error. A new alignment procedure which avoided these computations was developed and utilized for the alignment in this run. The final alignment was such that, due to the imperfection of the beam splitters, reflections from the artifact faces returned down the bore of the Lamb-dip stabilized laser, through an isolator, and coupled with the cavity oscil- lations. It was thus impossible to lock the laser automatically on this run and tuning to the Lamb dip was done manually before each measurement series.

The detector was also altered for this run, the metal mirrors were removed, and the shaft encoder, which was susceptible to electrical noise, was replaced with a precision wire wound pot, a D.C. power supply and digi- tal voltmeter. This device was much more stable than the encoder enabling us to track the phase reliably throughout the run. The exit beam from the

interferometer went straight to the quarter wave plate, then through the Faraday cell and the analyzer to the photodetector. Attempts at better quarter wave plate alignment were frustrated by wavefront mismatch (See Section VII).

Initial measurements in this run showed that the output beam non-orthogonality no longer depended upon the particular artifact but was constant at $\pm$ 2.44 $\pm$ .01 degrees independent of the artifact. This change in behavior was due presumably to one or all of the above changes in procedure.

Run AB was begun on 11/6/75 and terminated 11/25/75. Since the main purpose of this run was to check for temperature coefficients, the temperature was varied from 18 °C to 23 °C during the course of the run in a pseudorandom fashion. The data from the flat were used to compute the path mismatch in the interferometer from the pressure coefficient at constant temperature. This air path mismatch was .63 inches, the central path being longer. With this knowledge the remaining data were corrected for air pressure and air temperature effects and the resulting data used to compute the interferometer temperature coefficient. A linear least squares fit yielded a coefficient of 198.8 degrees (phase)/deg. C for the interferometer alone. This coefficient is much too large to come from any glass path mismatch or refractive index inhomogenities. We suspect that it originated at the beam splitter surfaces, which due to the performance degradation (also responsible for the "beam mixing") were operating in a very unstable portion of their response curve. [In a region of rapid change in the real part of a response function (transmission) the imaginary part (phase) is also rapidly changing, a phenomena well known to electrical engineers. It is necessitated by causality as expressed in the Kramers-Kronig relations.] We have performed no calculations to verify this hypothesis.

After the interferometer analysis the length differences between the artifacts as a function of temperature were linearly least squares fit to a straight line. The resulting coefficients were in reasonable agreement with the accepted values given in Table 1. The difference between the Homosil (H2) and the Cervit (C4T) was .54 $\pm$ .02 ppm/°C and the Cervit (C4T) and the Zerodur (Z7T) yielded .03 $\pm$ .02 ppm/°C. The large uncertainties reflect the narrow temperature range covered and the presence of non-random "beam mixing" errors. No attempt was made to remove these errors from the data set as the above results indicated that the anomously large temperature coefficients had been removed by one or all of the above changes, which was the purpose of this subsidiary experiment.

35

Conclusions

The main result of this project was an increased understanding of the polarization interferometer as an analytic and metrological tool. It seems clear from the preceding that if great care is taken measurements at the part in 10^8 or even 10^9 level will be possible with such instruments. To do this, however, will require construction of a new interferometer system based on the knowledge we have gained in this experiment.

The requirements of such a system are varied. For reasons of clarity we have outlined these requirements, as we currently conceive them, in Table 3.

Table 3. Outline of requirements for parts in 10^8 or 10^9 polarization interferometer.

I. Source

1) Source must be Lamb-dip stabilized or Iodine adsorption stabilized Helium-Neon laser for required frequency stability.

2) Laser must be effectively isolated from interferometer to prevent feedback.

3) Laser source must be spatially filtered and collimated to remove length dependent errors and allow for proper alignment. (Polarization differences caused by wavefront mismatch mask ellipticity effects.)

II. Mechanical Construction

1) Machinery for repositioning artifacts must be accurate and wear resistant. The previous specifications ($\pm$ 1 sec; $\pm$ .001 inches) seemed adequate but over-kill in this area would be highly desirable. The previous system did show measurable wear over a year's period, primarily due to damage of the flat used on the positioning plate.

2) In order to check the capability for absolute measurements and insure cleanliness it would be highly desirable to perform the measurements in a hard vacuum.

III. The Interferometer

1) Highly efficient stable beam splitters must be used.

2) Air and glass paths must be matched carefully for absolute measurements to be possible.

3) The number and type of thin film interface reflections and transmissions should be matched. This, with (2), should result in an interferometer with effectively zero ($<10^{-9}$/deg.C) temperature coefficient.

4) To avoid wavefront and polarization distortion the most homogeneous and least birefringent material available, perhaps fused silica, should be used throughout.

5) All retarders used in interferometer assembly should be of first order optically contacted quartz. This will yield greater band-

width, acceptance angle and temperature stability. This will also insure a reasonable match with interferometer expansion coefficients.

7) Whenever possible optics should be optically contacted, or coated to remove unwanted and confusing reflections.

8) Geometry must be such as to make measurements insensitive to angle to first order.

IV. The Detector

1) The birefringent quarter wave plate must be removed from the system since current state of the art precludes constructing these devices to better than 1% (about a 1° phase shift error). In its place a tunable Soleil-Babinet compensator or Fresnel Rhomb might be used.

2) The Faraday cell should be modified so that higher modualtion levels and greater transmission aperature are available. This will permit better noise rejection and allow a wider gauging area to be investigated.

3) It would be desirable to develop a means of spatially filtering the interferometer output before detection. This would allow the analysis of selected spatial frequency and thereby improve signal to noise and reduce wavefront matching requirements. This filtering might be conveniently done holographically.

4) Detector must include provisions to insure correct alignment of the retardation element used to produce circular polarization (see 1).

5) Analyzer must have a very high extinction ratio ($<10^4$) in order to check detector alignment and operation.

38

Bibliography

1. Memorandum of Agreement between Corning Glass Works and NBS on a Research Associate Program, CN-138 1972.

2. Cameron and Hailes, NBS Technical Note 844 (1974).

3. B. Justice, Report for NASA Contract NAS8-28662, January 10, 1975.

4. B. Justice, IARD Memo #74-320, September 10, 1974.

5. J. Dyson, Physica, Vol. 26, p532 (1958).
    F. Green, Optical Instruments and Techniques, 1969 (Conference Report) Oriel Press, Newcastle Upon Tyne, England, pg. 187.

6. Wm. Bruce Olsen, Optical Engineering 12, 3, 102 (1973).

7. H. Wenking, Z. Instrumentenk 66, 1 (1958).

8. Born and Wolf, "Principles of Optics", 5th Edition, Pergamon Press, N. Y. (1975).

Appendix A

Beam Coincidence Errors of the Dyson

Double-Pass Interferometer

by

A. W. Hartman

Dyson[1,2,3] has introduced an interferometer for the

measurement of thin films, which is characterized by two main

features:

(1) Insensitivity to small translations and rotations

of the specimen,

(2) signal output in the form of a polarization angle.

A diagram of this interferometer is shown in Figure 1.

Proper functioning of this instrument requires among other

things that the two output beams are parallel and coincident.

In practical instruments, this has often only partially been

achieved. [4]

In this note, beam coincidence errors are calculated

paraxially as a function of axial alignment and of prism con-

struction. The numbers have been taken from a prototype instru-

ment in operation at the Optical Physics Division of NBS.

The following parameters are studied:

(a) specimen thickness

(b) quarter-wave plate thickness

(c) distance of the beam-splitting point, and the reflecting

surface to the front focal plane of the lens

(d) distance of the specimen surface to the rear focal plane

(e) spherical aberation of the lens (in terms of % focal power)

(f) modification of the original cube-shaped Wollaston prism, with either one or the other polarized beam entering the interferometer normal to the prism surface.

The results of the calculations are in terms of "angle error" (=angle between output beams) and "spacing error" (=distance between beam exit points, assuming a very short polarizing prism). They have been plotted in Figures 2 and 3.

Several conclusions can be drawn:

(1) The beam-splitting point and reflector should be in the front focal plane, or optically symmetric on opposite sides of this plane

(2) the interferometer can be modified for measuring finite step heights by splitting the lens as shown in Figure 4. If only one step height value is of interest (such as the thickness of a specific gage block) and this value is fairly small relative to the focal length (15 - 20%), the lens can be of a cemented or even monolithic construction.

(3) The Wollaston prism has generally an appreciable beam "summation" error, which can be made zero by   slanting one of

the prism faces. In the particular case of a calcite/calcite prism with 14.2° cementing angle, the front face should be cut at a 20% slant, as shown in Figure 3. It is largely immaterial whether one or the other polarized beam exits normal to the prism.

More elaborate calculations are in progress to arrive at a complete model for the double-pass Dyson interferometer.

References

(1) J. Dyson, Physica 24 532 (1958).

(2) J. Dyson, Interferometry as a Measuring Tool, p. 96. The machinery Publishing Co.

(3) J. Dyson J. Opt. Soc. of Am. 53 690 (1963).

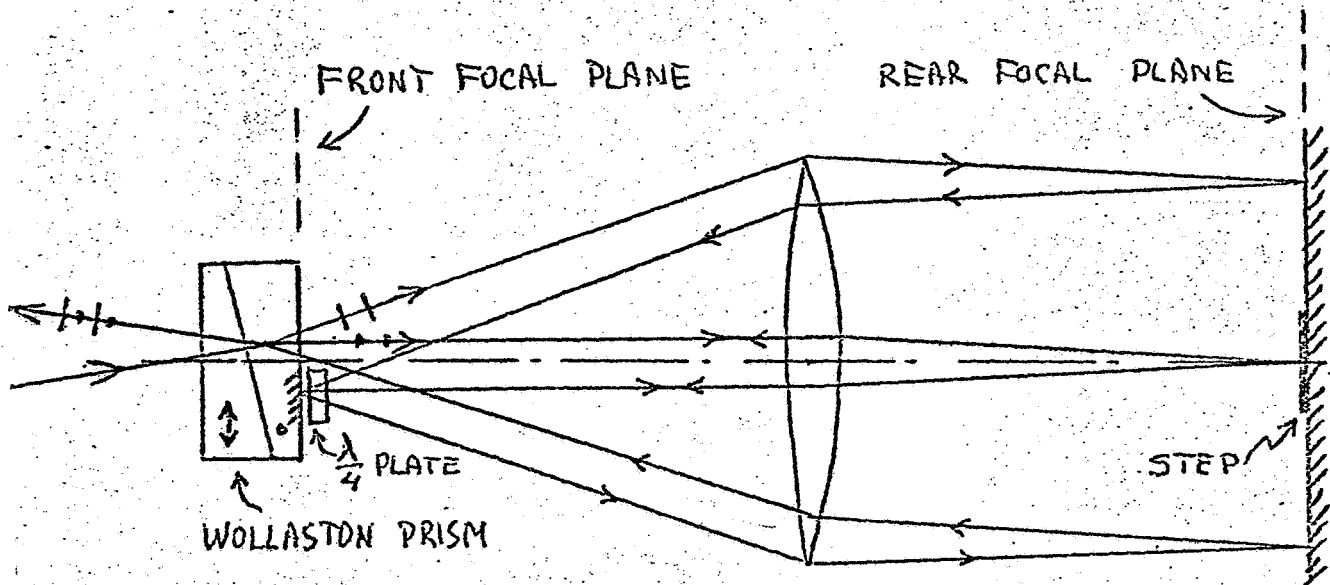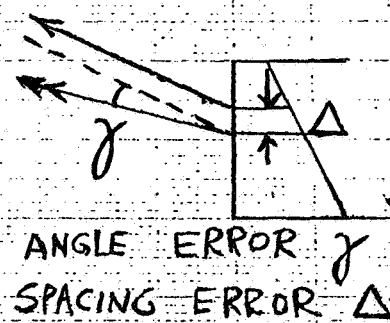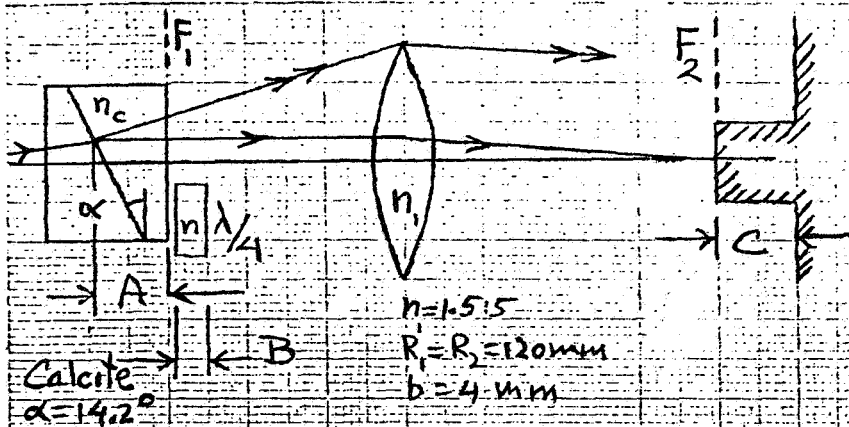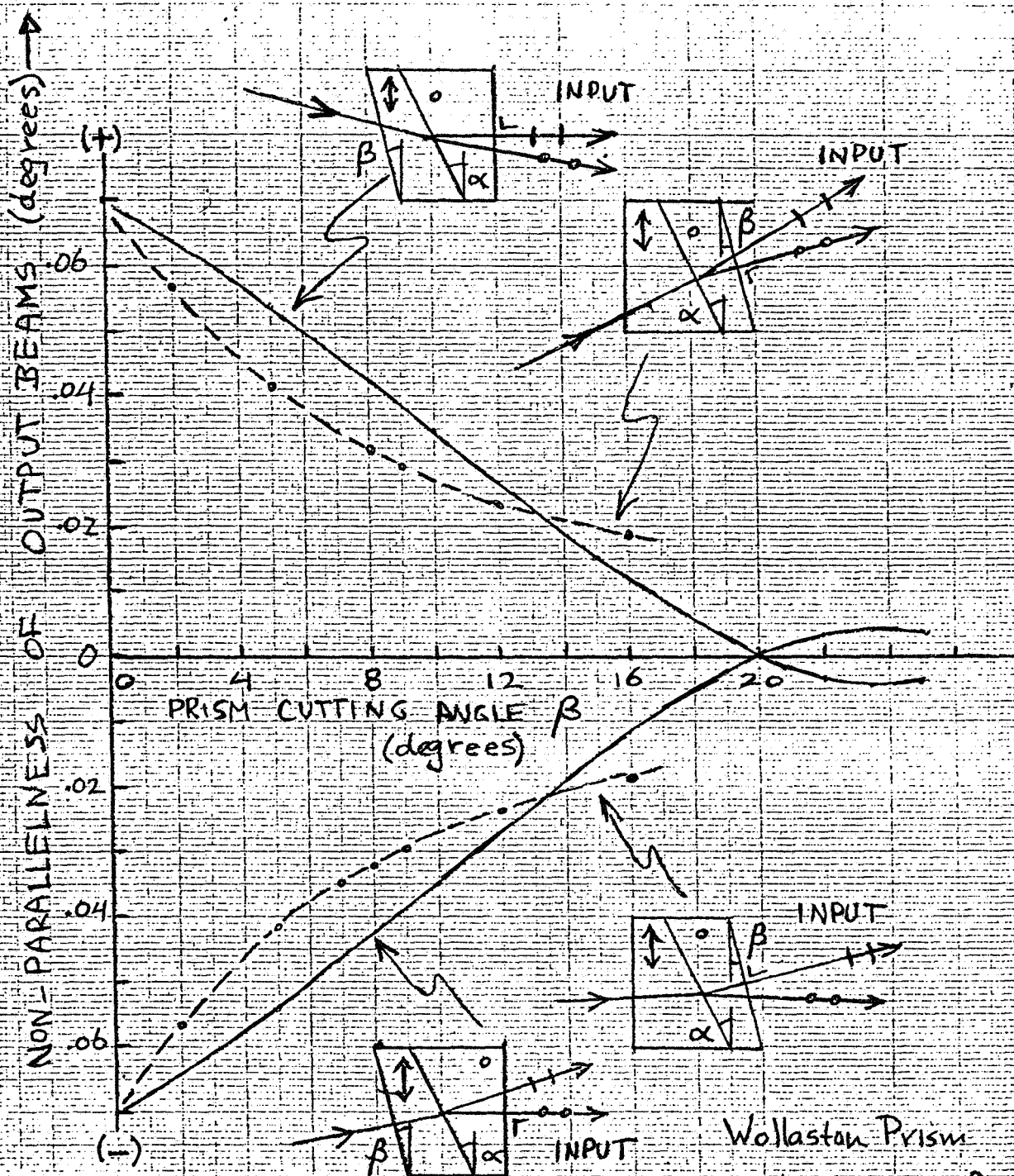(4) F. Green, Optical Instruments and Techniques 1969, J. H. Dickson Ed., p. 190.

FRONT FOCAL PLANE

REAR FOCAL PLANE

$\frac{\lambda}{4}$ PLATE

WOLLASTON PRISM

STEP

FIG.1

DYSON DOUBLE-PASS INTERFEROMETER

Top diagram labels:
F_1, n_c, α, $n\,\lambda/4$, n_1, F_2, C

A, B, Calcite $\alpha = 14.2°$

$n = 1.5.5$
$R_1 = R_2 = 120\,mm$
$b = 4\,mm$

ANGLE ERROR γ
SPACING ERROR Δ

γ

MISALIGNMENTS	Δ	γ
$A = B = 0$ $C = 0 \div 25\,mm \ (= X)$	$\Delta \leq 0.001\,mm$	$\gamma(rad)$ graph, 10^{-3}, 10^{-4} vs 10^{-2}, 10^{0} mm (X)
$\dfrac{A}{n_c} = \dfrac{B(n-1)}{n} = 0 \div 3\,mm \ (= X)$ $C = 0$	$\Delta(mm)$ graph 1.0, .5, 0 vs 0,1,2,3 mm (X)	$\gamma \leq 1 \times 10^{-5}\,rad$
$\dfrac{A}{n_c} = 0 \div 3\,mm \ (= X)$ $B = C = 0$	$\Delta(mm)$ graph 1.0, .5, 0 vs 0,1,2,3 mm (X)	$\gamma \leq 1 \times 10^{-6}\,rad$
$\dfrac{A}{n_c} = \dfrac{B(n-1)}{n} = 0 \div 2\,mm \ (= X)$ $C = 0$	$\Delta \leq 1 \times 10^{-4}\,mm$	$\gamma \leq 1 \times 10^{-7}\,rad$
Spherical Aberr. $\dfrac{F_{center} - F_{edge}}{F_{center}} = 0 \div 2\% \ (= X)$	$\Delta(mm)$ graph 1.0, .5, 0 "lens used" vs 0,1,2% (X)	$\gamma(rad)$ graph .002, .001 "lens used" vs 0,1,2% (X)

§2   ANGLE AND SPACING ERRORS VS MISALIGNMENTS

AWH

FIG. 3 ANGLE ERROR BETWEEN OUTPUT BEAMS
AS A FUNCTION OF PRISM CUTTING ANGLE

EDGE FOCAL PLANE

CENTER FOCAL PLANE

10.3mm   78.4 mm
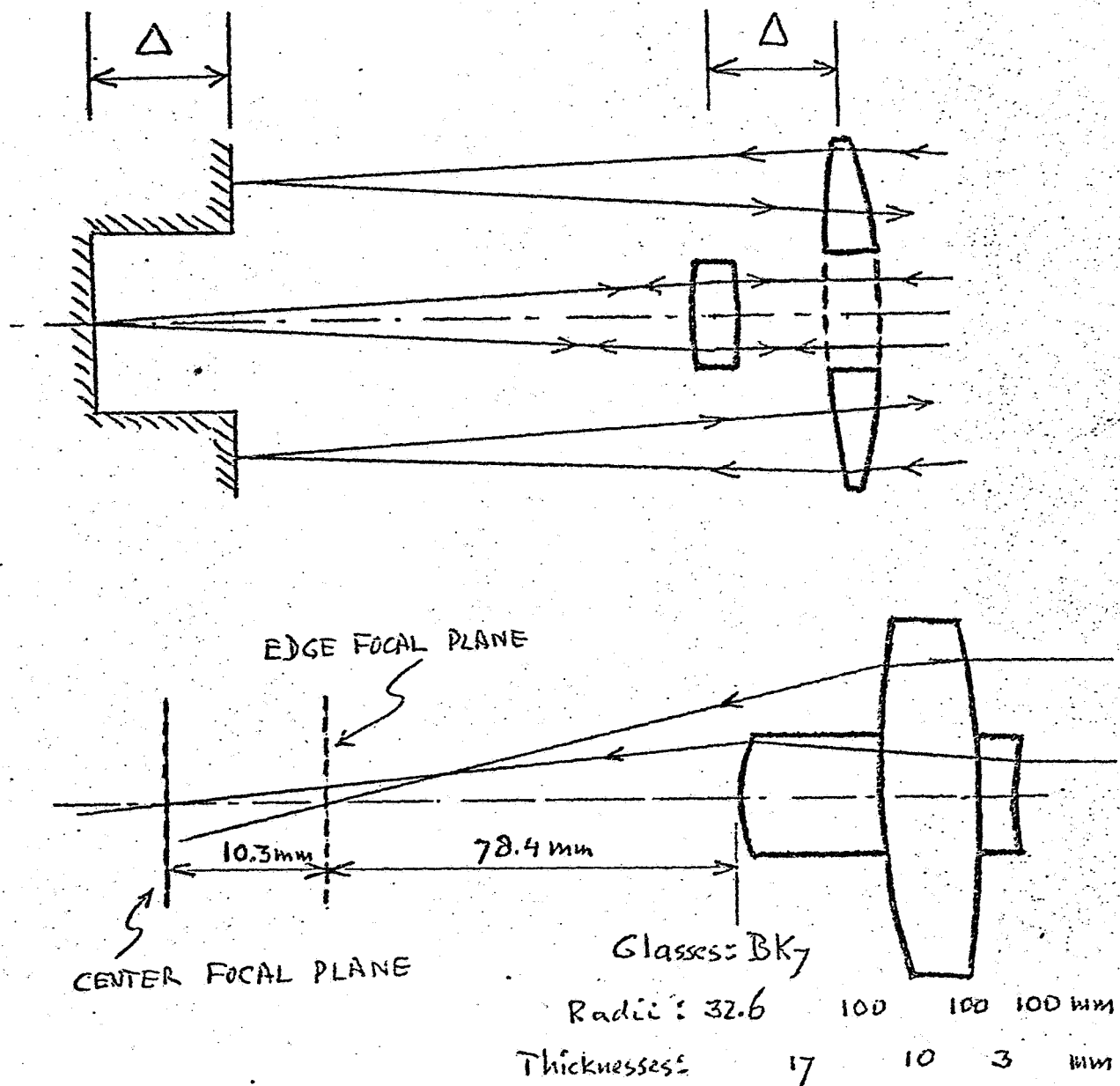
Glasses: BK7

Radii: 32.6   100   100 100 mm

Thicknesses: 17   10   3   mm

FIG.4   SPLIT-LENS DESIGN, FOR LARGE STEPS Δ

46